Active immunotherapy reduces NOTCH3 deposition in brain capillaries in a CADASIL mouse model

Oliveira, D.V.; Coupland, K.G.; Shao, W.C.; Jin, S.B.; Gaudio, F. del; Wang, S.L.; ... ; Karlstrom, H.

Citation

SOURCE DATA   TRANSPARENT PROCESS   OPEN ACCESS

Active immunotherapy reduces NOTCH3 deposition in brain capillaries in a CADASIL mouse model

Daniel V Oliveira[1,2,†] , Kirsten G Coupland[1,†] , Wenchao Shao[1], Shaobo Jin[1,3] , Francesca Del Gaudio[3] , Sailan Wang[1], Rhys Fox[1,3], Julie W Rutten[4], Johan Sandin[1,5,6], Henrik Zetterberg[7,8,9,10,11], Johan Lundkvist[1,5,12], Saskia AJ Lesnik Oberstein[4] , Urban Lendahl[1,3,*] & Helena Karlström[1,**]

Abstract

Cerebral autosomal dominant arteriopathy with subcortical infarcts and leukoencephalopathy (CADASIL) is the most common monogenic form of familial small vessel disease; no preventive or curative therapy is available. CADASIL is caused by mutations in the *NOTCH3* gene, resulting in a mutated NOTCH3 receptor, with aggregation of the NOTCH3 extracellular domain (ECD) around vascular smooth muscle cells. In this study, we have developed a novel active immunization therapy specifically targeting CADASIL-like aggregated NOTCH3 ECD. Immunizing CADASIL TgN3R182C[150] mice with aggregates composed of CADASIL-R133C mutated and wild-type EGF_{1-5} repeats for a total of 4 months resulted in a marked reduction (38–48%) in NOTCH3 deposition around brain capillaries, increased microglia activation and lowered serum levels of NOTCH3 ECD. Active immunization did not impact body weight, general behavior, the number and integrity of vascular smooth muscle cells in the retina, neuronal survival, or inflammation or the renal system, suggesting that the therapy is tolerable. This is the first therapeutic study reporting a successful reduction of NOTCH3 accumulation in a CADASIL mouse model supporting further development towards clinical application for the benefit of CADASIL patients.

Introduction

Cerebral autosomal dominant arteriopathy with subcortical infarcts and leukoencephalopathy (CADASIL, OMIN No. 125310) is the most common monogenic form of cerebral small vessel disease (SVD), affecting approximately 5/100,000 individuals, but is in all likelihood underdiagnosed (Rutten *et al*, 2016). Patients suffering from CADASIL experience migraine with aura, subcortical ischemic events, mood disturbances, apathy, and cognitive impairment (Joutel *et al*, 1996; Chabriat *et al*, 2009; Coupland *et al*, 2018; Joutel, 2020). CADASIL results in white matter lesions, neuronal loss, and widespread vascular pathology characterized by degenerating vascular smooth muscle cells (VSMC) and thickening of the arterial wall (fibrosis), which leads to lumen stenosis, for review see Coupland *et al* (2018).

Cerebral autosomal dominant arteriopathy with subcortical infarcts and leukoencephalopathy is exclusively caused by mutations in the *NOTCH3* gene (Joutel *et al*, 1996). The NOTCH3 transmembrane receptor undergoes proteolytic cleavages upon activation by ligands presented on juxtaposed cells, ultimately releasing the Notch intracellular domain (ICD) into the interior of the cell, while the Notch extracellular domain (ECD) is shed from the cell surface (see Fig 1A for details on Notch signaling) (Andersson *et al*, 2011;

1 Department of Neurobiology, Care Sciences and Society, Karolinska Institutet, Stockholm, Sweden
2 Department of Cell Biology, Faculty of Science, Charles University, Prague, Czech Republic
3 Department of Cell and Molecular Biology, Karolinska Institutet, Stockholm, Sweden
4 Department of Clinical Genetics, Leiden University Medical Center, Leiden, The Netherlands
5 Alzecure Foundation, Huddinge, Sweden
6 Alzecure Pharma, Huddinge, Sweden
7 Department of Psychiatry and Neurochemistry, Institute of Neuroscience and Physiology, The Sahlgrenska Academy at the University of Gothenburg, Mölndal, Sweden
8 Clinical Neurochemistry Laboratory, Sahlgrenska University Hospital, Mölndal, Sweden
9 Department of Neurodegenerative Disease, UCL Institute of Neurology, Queen Square, London, UK
10 UK Dementia Research Institute at UCL, London, UK
11 Hong Kong Center for Neurodegenerative Diseases, Clear Water Bay, Hong Kong, China
12 Sinfonia Biotherapeutics, Huddinge, Sweden
   *Corresponding author. Tel: +46 (0)8 524 873 23; E-mail: urban.lendahl@ki.se
   **Corresponding author. Tel: +46 (0)8 524 835 48; E-mail: helena.karlstrom@ki.se
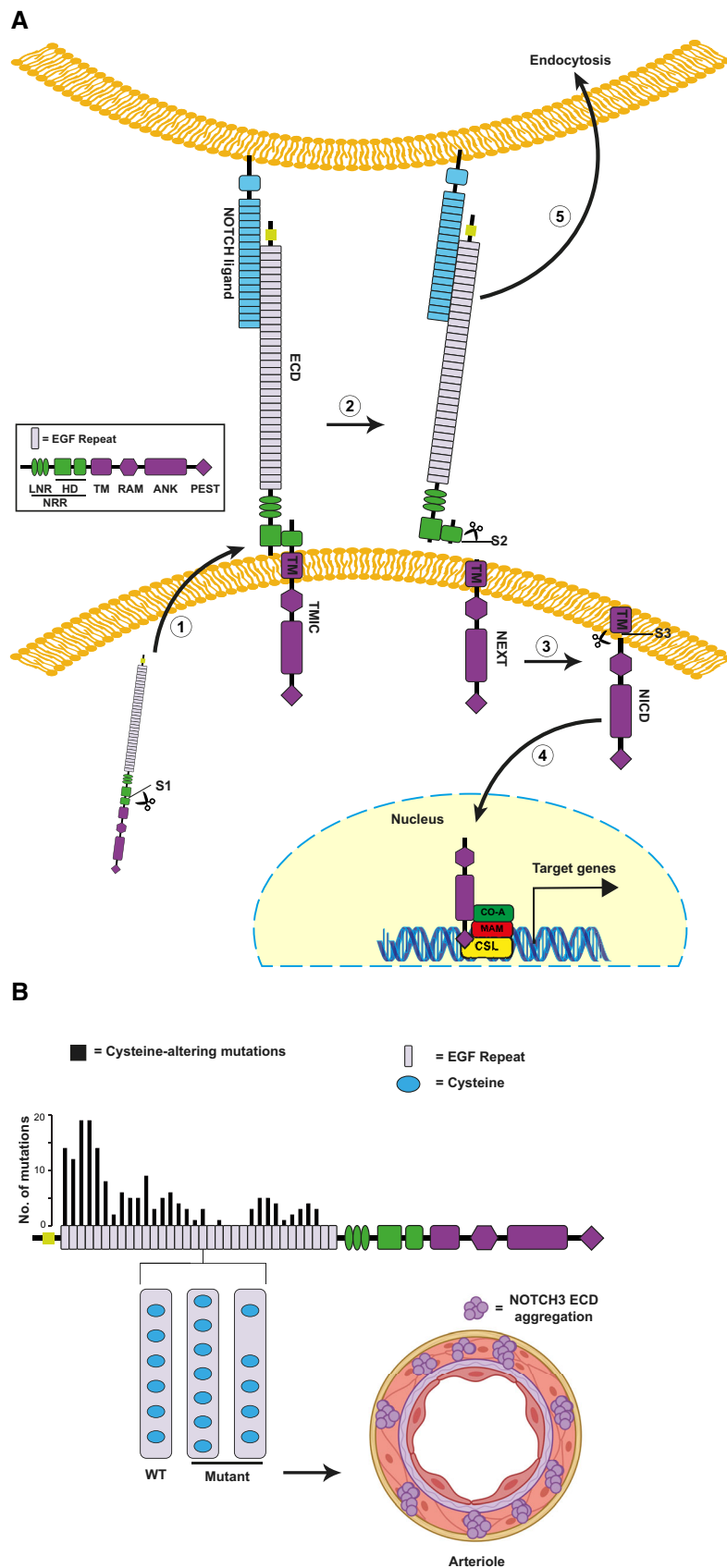   †These authors contributed equally to this work as first authors

Figure 1.

Figure 1. Schematic representation of Notch signaling and Notch3 CADASIL mutations.

A Schematic representation of Notch signaling. (1) Furin (S1 cleavage) cleaves the NOTCH3 precursor protein in the Golgi system, resulting in a non-covalently bound bipartite protein that is transported to the cell surface. (2) A mechanical traction force is applied to the NOTCH3 ECD when a Notch ligand binds to the EGF repeats 10–11, exposing the extracellular NRR near the cell membrane, which consists of LNR and the heterodimerization domain (in green). Subsequently, ADAM17 cleaves the C-terminal portion of the heterodimerization domain (S2-cleavage). (3) The NEXT, which is made up of a RAM domain, the ANK domains, a PEST domain, and a transmembrane domain, is cleaved by the γ-secretase (S3-cleavage) releasing the N3ICD. (4) The N3ICD binds to the CSL protein and together with the co-activator Mastermind-like (MAM) trigger downstream gene transcription in the nucleus. (5) The NOTCH3 ECD and ligand are normally endocytosed by the ligand-expressing cell and degraded in the lysosome.

B Schematic representation of NOTCH3 cerebral autosomal dominant arteriopathy with subcortical infarcts and leukoencephalopathy (CADASIL) mutations. NOTCH3 ECD contains 34 EGF repeat domains, each of which has six cysteine residues (WT). Mutations in CADASIL change the number of cysteines to an uneven number of cysteines (Mutant). These unpaired cysteines residues result in incorrect EGF repeat folding, irregular protein folding which leads to an enhanced NOTCH3 ECD multimerization. Distribution of the cysteine-altering mutations that cause CADASIL are shown. In the CADASIL mutant NOTCH3 ECD, the endocytosis is hampered, and NOTCH ECD remains outside of the VSMC and starts to accumulate and aggregate around the vessels. ADAM17, a disintegrin and metalloproteinase domain-containing protein 17; ANK, ankyrin repeats; EGF, epidermal growth factor; HD, heterodimerization domain; LNR, Lin-Notch repeats; PEST, proline (P), glutamic acid (E), serine (S), and threonine (T) degradation domain; RAM, Rbp-associated molecule domain; TM, transmembrane domain.

Siebel & Lendahl, 2017; Coupland et al, 2018). Most CADASIL mutations are missense mutations confined to the 34 epidermal growth factor (EGF)-like repeats of the NOTCH3 ECD moiety (Rutten et al, 2014), resulting in an altered number of cysteine residues in the EGF-like repeats (Fig 1B; Joutel et al, 1996). The CADASIL cysteine-altering mutations perturb the structure of NOTCH3 ECD resulting in NOTCH3 ECD multimerization and aggregation. This in turn leads to the recruitment of microvascular extracellular matrix proteins including metalloproteases and vitronectin, that form the so called granular osmiophilic dense material, GOM, a histopathological hallmark of CADASIL (Karlstrom et al, 2002; Duering et al, 2011; Monet-Lepretre et al, 2013; Capone et al, 2016; Fig 1B). NOTCH3 ECD accumulation is one of the earliest events in CADASIL pathogenesis, indicating that it may cause cellular pathology by inducing changes in the brain microvascular extracellular matrix (Joutel et al, 2001, 2010; Monet-Lepretre et al, 2013; Capone et al, 2016). Collectively, these data argue that CADASIL may be considered a protein misfolding and aggregation disease.

There are currently no therapies to abrogate or ameliorate the disease process for CADASIL patients but given that NOTCH3 accumulation is a hallmark of the disease, immunotherapy targeting NOTCH3 aggregation or aggregates may be an attractive therapeutic strategy. Immunotherapeutic approaches are gaining increasing attention as novel disease modifying therapies for protein misfolding and aggregation diseases such as certain neurodegenerative diseases (Forman et al, 2004; Shrivastava et al, 2017). Promising preclinical and clinical results have been obtained in particular for the clearance of amyloid beta (Aβ) deposits (the so called "senile plaques") in Alzheimer's disease (AD). Therapies based on both active and passive immunization can clear amyloid in the brain with great efficiency in preclinical mouse models of Aβ amyloidosis as well as in patients. Recently, a number of different monoclonal antibodies targeting Aβ aggregates have demonstrated promising clinical improvement in association with amyloid clearance in Phase II and III clinical trials with aducanumab recently being approved for treatment of AD by the Food and Drug Association (Budd Haeberlein et al, 2017; Tolar et al, 2020; Mintun et al, 2021). Although the efficacy of the compound has been questioned and challenged (Knopman et al, 2021), this passive vaccine is still of interest not only for the AD field but also encourages development of immunotherapies for other disorders where protein misfolding and aggregation are believed to play a pivotal pathological role.

Cerebral autosomal dominant arteriopathy with subcortical infarcts and leukoencephalopathy shares a number of features with AD, including that both are considered protein misfolding and aggregation diseases and that both NOTCH3 and Aβ aggregates accumulate in the extracellular milieu. It is thus conceivable that NOTCH3 aggregates are accessible to efficient antibody-mediated clearance, as has been demonstrated for Aβ immunotherapies. Thus far, passive immunization has been explored in pre-clinical CADASIL mouse models with potentially encouraging results (Machuca-Parra et al, 2017; Ghezali et al, 2018), including ameliorative effects on cerebrovascular dysfunctions such as impaired blood flow and myogenic tone, although no attenuation of NOTCH3 ECD or GOM deposition was observed (Ghezali et al, 2018). To directly target the NOTCH3 ECD aggregation, it may therefore be interesting to explore an active immunization strategy, a therapeutic strategy which has been proven safe in several AD trials with different vaccines targeting Aβ (Vandenberghe et al, 2017; Novak et al, 2019; Rosenberg & Lambracht-Washington, 2020). Active immunization may be particularly appealing as a treatment for CADASIL for a number of reasons. First, the NOTCH3 deposits are located in the vessel walls and thus readily accessible to the circulating humoral immune defense enabling efficient NOTCH3 aggregate targeting. Second, given the dominant nature and high penetrance of the NOTCH3 mutations, a large number of CADASIL patients and CADASIL mutation carriers could be identified at a young age, when an active immunization has a greater potential to mount an efficient immune response. Finally, CADASIL is a chronic life-long disease and vaccine injections restricted to a few times yearly, as opposed to monthly or even more frequently, which could be the case with passive vaccines, would be advantageous from a patient perspective.

In this study, we report on the development of an active immunization therapy aimed at targeting the CADASIL-associated NOTCH3 pathology as a novel disease-modifying therapy for the treatment of CADASIL. We take advantage of a CADASIL mouse model (TgN3R182C^{150}), which expresses a human NOTCH3 R182C receptor and which develops a progressive cerebrovascular NOTCH3 ECD and GOM deposition phenotype in arterioles (Rutten et al, 2015), and thus is a suitable preclinical model for the development of therapies targeting CADASIL-associated NOTCH3 pathology. We find that active repeated immunization starting at 3 months of age results in reduced NOTCH3 ECD deposition around

capillaries and lowered levels of NOTCH3 ECD in the blood at 7 months of age, which was the end point of the experiments. No loss of VSMC in the retina, and no inflammation, neuronal or kidney damage was observed after NOTCH3 immunization, indicating that the active immunotherapy does not alter normal Notch signaling. Collectively, the data suggest that active immunization that specifically targets aggregated NOTCH3 may be an efficacious and tolerable therapeutic strategy for CADASIL therapy development.

Results

Production of recombinant N3 EGF$_{1-5}$ antigen for active immunization

To perform active immunization in the CADASIL TgN3R182C^{150} mouse model, we first generated a suitable antigen, that would be selective for aggregated NOTCH3 and spare monomeric NOTCH3 receptors, potentially minimizing adverse effects on NOTCH3 signaling. To this end, we produced an immunogen based on aggregates of the NOTCH3 EGF repeat (EGF$_{1-5}$), the part of NOTCH3 which contains the majority of all CADASIL-causing mutations identified to date. Although using a mouse model carrying the NOTCH3 R182C mutation, we opted for another cysteine-altering mutation (NOTCH3 R133C) for generation of the aggregated antigen, since this protein previously has been shown to generate aggregates and represents a mutation in the "hot-spot" region in the NOTCH3 protein (EGF$_{1-6}$), but also to determine whether an aggregation-general rather than a mutation-specific therapy could be efficacious. By mixing the NOTCH3 EGF$_{1-5}$ R133C with wild-type (WT) NOTCH3 EGF$_{1-5}$, we obtained excellent *in vitro*-aggregation, in line with previous reports (Opherk *et al*, 2009; Duering *et al*, 2011), which would increase the chances of producing an immunogenic aggregate. From stable cells lines producing NOTCH3 EGF$_{1-5}$ from either WT or NOTCH3^{R133C}, we purified poly-histidine- and c-Myc-tagged NOTCH3 EGF$_{1-5}$ WT or NOTCH3^{R133C} fragments (Duering *et al*, 2011) from cell culture medium by metal ion affinity chromatography capturing the poly-histidine tag (Fig 2A). This resulted in a yield of approximately 90% of the total protein content in the aggregated form (Fig 2B). We next explored the potential of the NOTCH3 EGF$_{1-5}$ peptides to multimerize and produce an amorphous aggregate (Duering *et al*, 2011) by incubating equal amounts of WT with R133C fragments or the WT and R133C fragments separately at 37°C for 5 days. Spontaneous multimer aggregation increased with time of incubation, which is in line with previous observations (Opherk *et al*, 2009; Duering *et al*, 2011), with a prominent loss of monomeric NOTCH3 EGF$_{1-5}$ when WT and R133C fragments were mixed when compared with incubating them separately (Fig 2C). Aggregates from mixed WT and R133C (WT/R133C aggregates) were therefore selected for the active immunization experiments.

N3 EGF$_{1-5}$ antigen evokes a robust immune response in TgN3R182C^{150} mice

We next assessed the immunogenic potential of the aggregated NOTCH3 EGF$_{1-5}$ peptides and whether they could prevent NOTCH3 ECD aggregation. Active vaccination was initiated at 3 months of age, 2 months before NOTCH3 protein accumulation is observed in the TgN3R182C^{150} mice (Rutten *et al*, 2015). Aggregated NOTCH3 EGF$_{1-5}$ WT/R133C protein plus adjuvant (with PBS plus adjuvant as sham-immunization control) was used to immunize TgN3R182C^{150} mice at 3 months of age (Fig 3A; Kontsekova *et al*, 2014). A booster shot containing aggregated protein plus adjuvant, or PBS plus adjuvant as control, was administered 1 month later. Two weeks later, another booster shot containing only NOTCH3 EGF$_{1-5}$ WT/R133C protein or PBS was injected, and further booster shots were administered every 2 weeks until 7 months of age, which was the end point of the analysis (Fig 3A; Kontsekova *et al*, 2014). Using a NOTCH3 EGF$_{1-5}$ aggregate ELISA, we assessed the immune response in the serum of the immunized mice at 1, 2- and 4-month post-immunization, i.e., at 4, 5, and 7 months of age. We observed a progressive increase in the immune response of the vaccinated versus the sham-immunized mice at 1- and 2-month post-vaccination and the increase was further pronounced at 4-month post-vaccination (Fig 3B). In conclusion, these data show that an immune response is mounted against the injected NOTCH3 EGF$_{1-5}$ WT/R133C aggregates.

The numbers and size of NOTCH3 ECD deposits around capillaries are reduced in NOTCH3 EGF$_{1-5}$ WT/R133C-vaccinated TgN3R182C^{150} mice

We first determined whether active immunization resulted in lower levels of NOTCH3 ECD deposition in the TgN3R182C^{150} brain vasculature. Brain tissue from NOTCH3 EGF$_{1-5}$ WT/R133C-vaccinated TgN3R182C^{150} mice as well as from sham-vaccinated or untreated TgN3R182C^{150} controls was processed for NOTCH3 ECD immunohistochemistry. NOTCH3 ECD deposits have mostly been described to occur in small arteries/arterioles. To assess NOTCH3 accumulation in arteries/arterioles, we stained for NOTCH3 and alpha-smooth muscle actin (ASMA), the latter a marker for VSMC in arteries/arterioles (Vanlandewijck *et al*, 2018). The notion that ASMA staining is confined to arteries/arterioles was corroborated by analysis of isolated brain microvessels from the TgN3R182C^{150} and WT C57Bl6/J mice, demonstrating that ASMA only stains VSMC in arteries/arterioles but not pericytes in capillaries, as determined by Perlecan, PDGFRβ and NG2 staining (Fig EV1). We observed a significant increase in both the percentage ($P = 0.0046$) and the number ($P = 0.0069$) of NOTCH3 deposits per vessel area as well as the average size of the deposits ($P = 0.0009$) in the non-treated 18 months when compared with 7-month-old TgN3R182C^{150} mice (Fig 4A and B), in keeping with a previous report (Rutten *et al*, 2015). The increase in NOTCH3 deposition was not linked to increased expression of the NOTCH3 gene, as no differences in expression of NOTCH3 and three downstream target genes (*Hes1*, *Hey1* and *Nrip2*) were observed during aging of the TgN3R182C^{150} mice (Fig EV2). We did not observe a difference in NOTCH3 ECD deposition in arteries/arterioles between the non-vaccinated, sham-vaccinated and vaccinated TgN3R182C^{150} mice at 7 months of age. There are several explanations as to why this might be the case. One explanation is that NOTCH3 ECD deposition in arteries/arterioles is not affected by the vaccination. Alternatively, NOTCH3 ECD deposition may start after 7 months of age in arteries/arterioles in this mouse model or deposit levels were too low to be successfully abrogated at 7 months of age (Fig 4A and B).
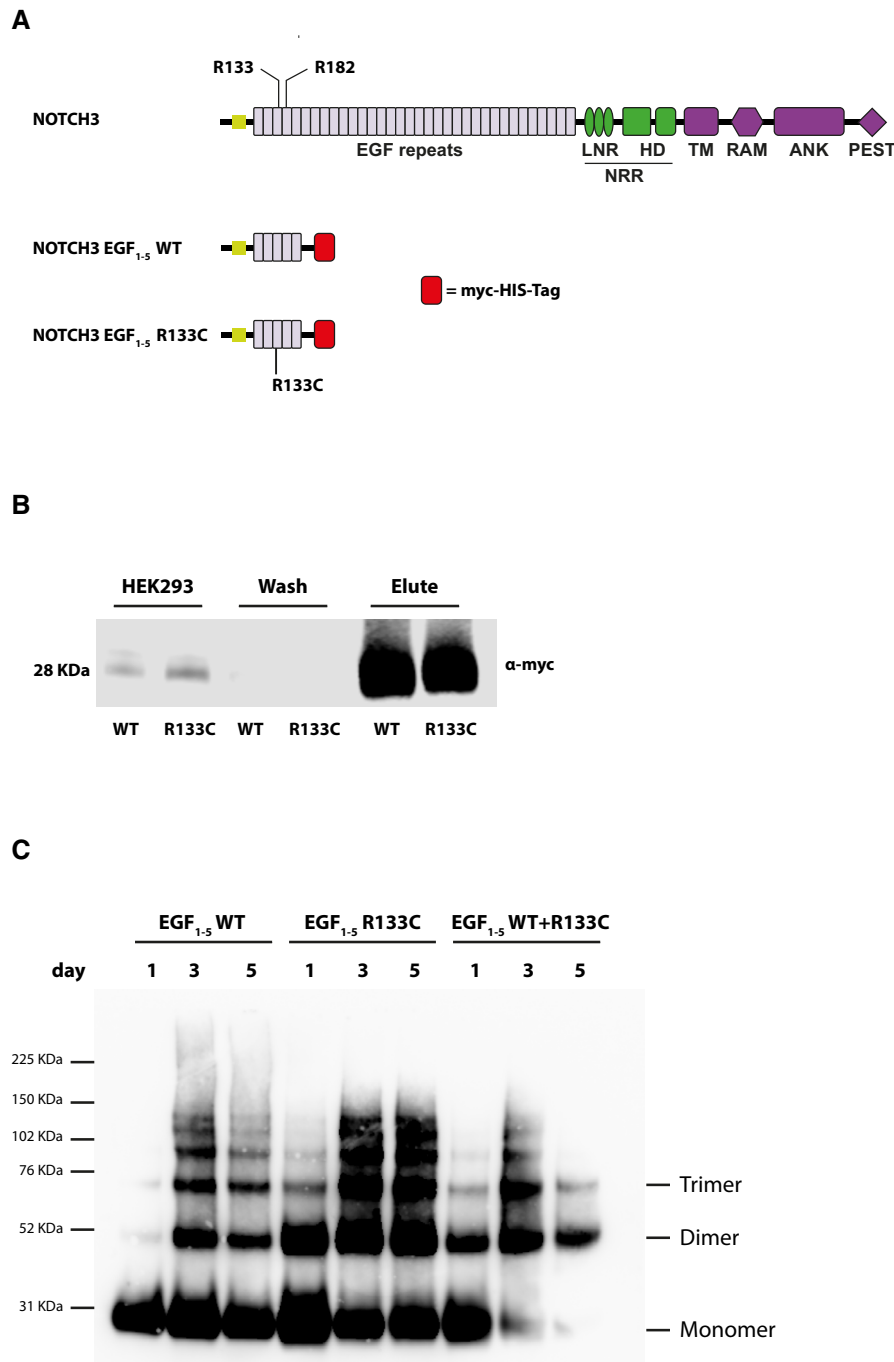
Figure 2. Schematic representation of NOTCH3 and NOTCH3 EGF$_{1-5}$ proteins and NOTCH3 EGF$_{1-5}$ antigen purification.

A Schematic representation of NOTCH3 and NOTCH3 EGF$_{1-5}$. NOTCH3 represents the full-length protein, and NOTCH3 EGF$_{1-5}$ represents the NOTCH3 protein with exon 1–5 fused with a myc-His-Tag at the C-terminus used for purification of the aggregated protein.

B Western blot of the NOTCH3 EGF$_{1-5}$ WT and R133C purified proteins. The eluate fractions were visualized by western blot using an α-myc antibody.

C Western blot of NOTCH3 EGF$_{1-5}$ WT and R133C aggregated proteins. The incubated fractions of NOTCH3 EGF$_{1-5}$ WT and R133C were visualized on a western blot using an α-myc antibody. The purified proteins and the aggregates were visualized after 1–5 days incubation by western blot using α-myc antibody under non-reducing conditions.

Source data are available online for this figure.

Given the extensive deposition of NOTCH3 aggregates around capillaries in CADASIL (Yamamoto *et al*, 2013), we next assessed differences in NOTCH3 deposition in the capillaries by using a combination of NOTCH3 and perlecan immunohistochemistry, as perlecan stains the basement membrane around both arteries and capillaries. We found increased NOTCH3 deposition as a percentage
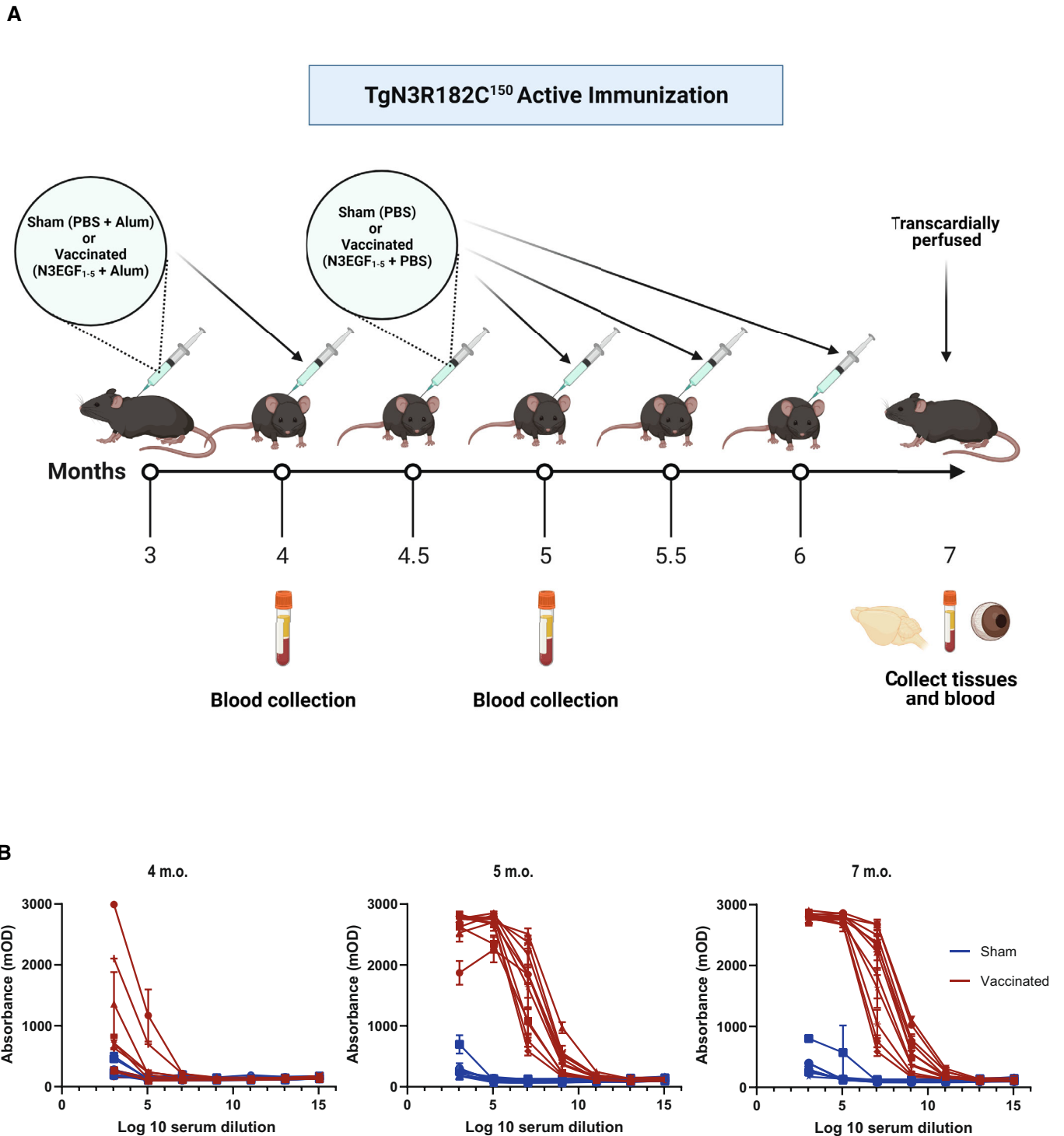
Figure 3. NOTCH3 EGF$_{1-5}$ antigen evokes a robust immune response in TgN3R182C^{150} mice.

A   Schematic pipeline of the subcutaneous active immunization in the TgN3R182C150 mouse model.

B   Antibody titer validation of serum from TgN3R182C150 CADASIL mice immunized with NOTCH3 EGF$_{1-5}$ aggregates (vaccinated, $n = 11$) and PBS (sham, $n = 9$) at 4, 5, and 7 months old. A direct ELISA with NOTCH3 aggregate-coated plates and different dilutions of serum was performed. Error bars indicate standard error of the mean (SEM).
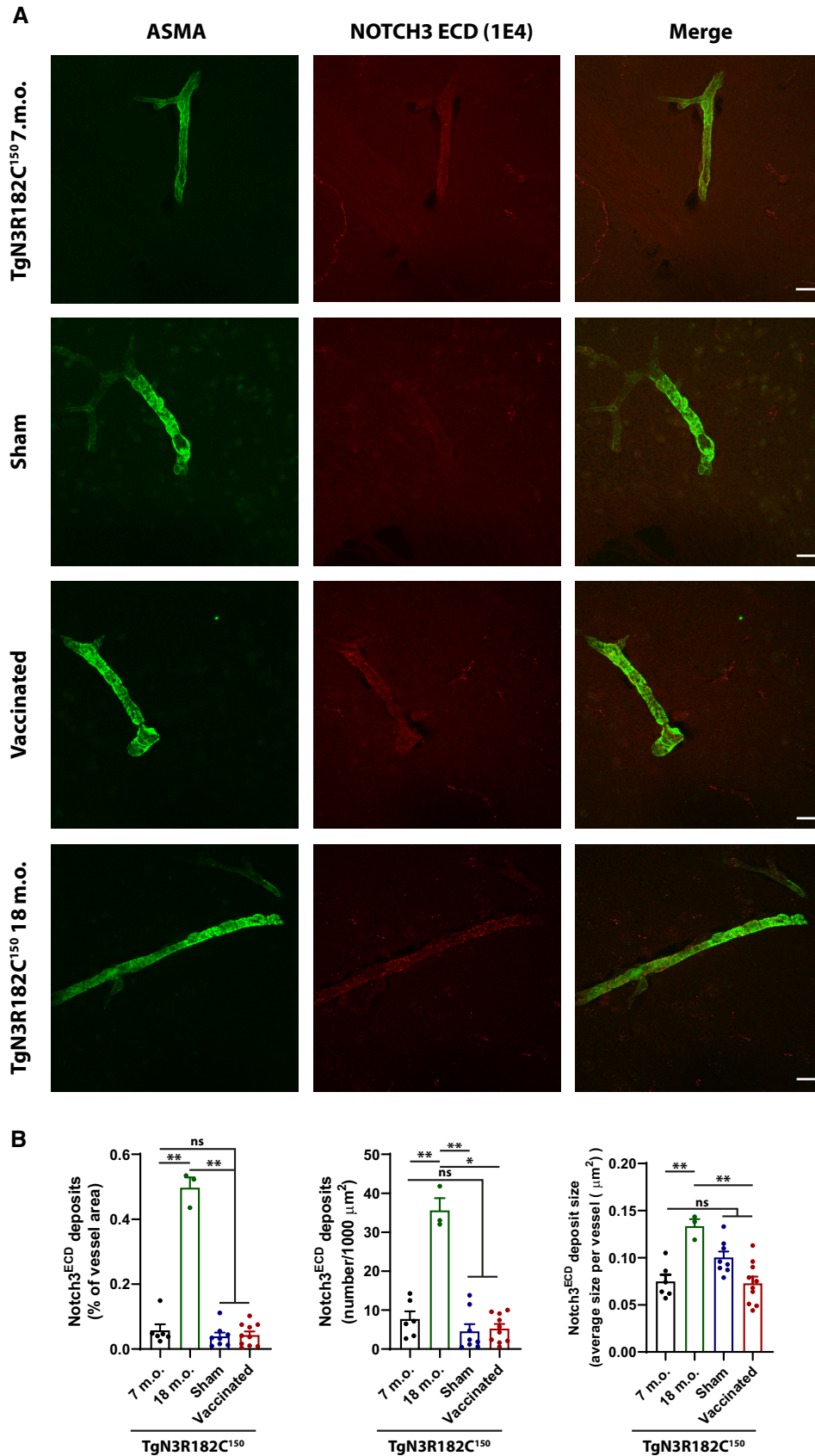
Figure 4.

Figure 4. NOTCH3 ECD and alpha-smooth muscle Actin (ASMA) expression in cerebral arteries/arterioles.

A Representative images of TgN3R182C150, sham- and NOTCH3 EGF$_{1-5}$-immunized mice at 7 months of age and TgN3R182C150 at 18 months of age. Representative images show brain arteries of TgN3R182C150 (7 and 18 months), sham and NOTCH3 EGF$_{1-5}$-immunized mice stained with a monoclonal antibody against NOTCH3 ECD (1E4, red) and an α-SMA antibody (green). Scale bar = 20 μm.

B Quantification of NOTCH3 ECD deposits (numbers per 1,000 μm^2) and NOTCH3 ECD stained area and average size per vessel revealed no decrease in NOTCH3 ECD deposition in brain arteries between NOTCH3 EGF$_{1-5}$-immunized ($n = 10$), sham ($n = 8$), and non-vaccinated ($n = 6$) TgN3R182C150 mice at 7 months of age. NOTCH3 ECD deposits (numbers per 1,000 μm^2) and NOTCH3 ECD stained area and average size per vessel increases significantly in the TgN3R182C150 mice at 18 months ($n = 3$) of age versus NOTCH3 EGF$_{1-5}$-immunized ($n = 10$), sham ($n = 8$), and non-vaccinated ($n = 6$) TgN3R182C150 mice at 7 months of age. Statistical significance was assessed using a Brown-Forsythe and Welch ANOVA tests followed by Dunnett's T3 multiple comparisons (NOTCH3 ECD deposits (% of vessel area): 7 m.o. vs. Sham, ns $P = 0.9424$; 7 m.o. vs. Vaccinated, ns $P = 0.9809$; 7 m.o. vs. 18 m.o. $^{**}P = 0.0046$; Sham vs. Vaccinated, ns $P = 0.9999$; Sham vs. 18 m.o. $^{**}P = 0.0032$; Vaccinated vs. 18 m.o. $^{**}P = 0.0032$. NOTCH3 ECD deposits (number/1,000 μm^2): 7 m.o. vs. Sham, ns $P = 0.7877$; 7 m.o. vs. Vaccinated, ns $P = 0.8358$; 7 m.o. vs. 18 m.o. $^{**}P = 0.0069$; Sham vs. Vaccinated, ns $P = 0.9995$; Sham vs. 18 m.o. $^{**}P = 0.0044$; Vaccinated vs. 18 m.o. $^{*}P = 0.0104$). NOTCH3 ECD deposits size: 7 m.o. vs. Sham, ns $P = 0.1169$; 7 m.o. vs. Vaccinated, ns $P > 0.9999$; 7 m.o. vs. 18 m.o. $^{***}P = 0.0009$; Sham vs. Vaccinated, ns $P = 0.0577$; Sham vs. 18 m.o. $^{**}P = 0.007$; Vaccinated vs. 18 m.o. $^{****}P < 0.0001$, ns = non-significant). Error bars indicate standard error of the mean (SEM).

Source data are available online for this figure.

of capillary vessel area ($P = 0.0029$), number of deposits per 1,000 μm^2 of capillary vessel area ($P = 0.0038$), as well as NOTCH3 ECD deposit size ($P = 0.0215$; Fig 5A and B) in 18-month-old non-treated TgN3R182C^{150} mice compared with their 3 months counterparts. In contrast to the arteries/arterioles, the increase in the number of NOTCH3 ECD deposits ($P = 0.001$) and percentage of deposits per vessel area ($P < 0.0001$) around capillaries was abrogated in vaccinated TgN3R182C^{150} mice, while no corresponding reductions were noted in the sham-vaccinated TgN3R182C^{150} mice at 7 months (Fig 5A and B). Similarly, the average size of NOTCH3 ECD deposits in the vaccinated TgN3R182C^{150} mice was decreased when compared with non-treated or sham-vaccinated mice ($P = 0.0038$; Fig 5A and B). In conclusion, these data demonstrate that active immunization with NOTCH3 EGF$_{1-5}$ WT/R133C aggregates specifically reduces the amount of NOTCH3 aggregates around cerebral capillaries.

The amount of NOTCH3 ECD is reduced in blood from NOTCH3 EGF$_{1-5}$ WT/R133C-vaccinated TgN3R182C^{150} mice

Elevated levels of NOTCH3 ECD in the blood have been observed in a CADASIL mouse model and in plasma and serum from CADASIL patients (Primo *et al*, 2016). We therefore wanted to extend the analysis of active immunization to learn whether NOTCH3 ECD blood levels were also altered in the CADASIL mouse model. To assess this, we first measured the levels of NOTCH3 ECD in blood

from TgN3R182C^{150} mice using an ELISA assay adapted from a previous report (Primo *et al*, 2016). NOTCH3 ECD was detected in whole blood serum of non-treated TgN3R182C^{150} mice at 3 months of age and at elevated levels at 7 months of age ($P = 0.0093$; Fig 6A). In contrast, no signal above the background was detected in C57BL/6 WT mice or in Notch3$^{-/-}$ mice at 7 months of age (Fig 6A). Serum NOTCH3 ECD in vaccinated TgN3R182C^{150} mice was significantly reduced compared with sham-vaccinated animals ($P = 0.0196$; Fig 6B). To exclude that the observed reduction of NOTCH3 ECD in the serum was a consequence of competition between the capture antibody in the ELISA and the raised humoral response by the vaccination, we added serum from sham or vaccinated C57BL6/J WT mice to the serum samples from TgN3R182C^{150} mice in 1:1 dilution. No difference in the NOTCH3 ECD levels was observed after dilution normalization (Fig EV3), suggesting that there was no interference between the humoral response and the ELISA capture antibody. Collectively, these data show that active immunization with aggregated NOTCH3 EGF$_{1-5}$ WT/R133C reduces the amount of circulating NOTCH3 ECD in serum in the TgN3R182C^{150} CADASIL mouse model.

The number of activated microglia is increased in NOTCH3 EGF$_{1-5}$ WT/R133C-vaccinated TgN3R182C^{150} mice

Microglia are the innate immune cells of the brain and play an important role in phagocytosis of aggregates in the brain (Rogers

Figure 5. NOTCH3 ECD and perlecan expression in cerebral capillaries.

A Representative images of TgN3R182C150, sham- and NOTCH3 EGF$_{1-5}$-immunized mice at 3, 7 and 18 months of age. Representative images show brain arteries and capillaries of TgN3R182C150, sham and NOTCH3 EGF$_{1-5}$-immunized mice stained with a monoclonal antibody against NOTCH3 ECD (1E4, red) and an anti-perlecan antibody (green). Scale bar = 20 μm.

B Quantification of NOTCH3 ECD deposits (numbers per 1,000 μm^2) and NOTCH3-ECD stained area and average size per vessel revealed a significant increase in NOTCH3 ECD deposition in brain arteries and capillaries between non-vaccinated 3-month-old TgN3R182C150 ($n = 3$) and 7-month-old TgN3R182C150 ($n = 6$) mice and 18-month-old TgN3R182C150 ($n = 3$). Quantification of NOTCH3-ECD deposits (numbers per 1,000 μm^2) and NOTCH3-ECD stained area and average size per vessel revealed a significant decrease in NOTCH3-ECD deposition in brain arteries and capillaries between NOTCH3 EGF$_{1-5}$-immunized ($n = 11$), sham ($n = 8$), and non-vaccinated TgN3R182C150 ($n = 6$) mice. Statistical significance was assessed using a Brown-Forsythe and Welch ANOVA tests followed by Dunnett's T3 multiple comparisons (NOTCH3 ECD deposits (% of vessel area): 3 m.o. vs. 18 m.o. $^{**}P = 0.0029$; 3 m.o. vs. 7 m.o. $^{***}P = 0.0004$; 7 m.o. vs. Sham, ns $P = 0.7326$; 7 m.o. vs. Vaccinated, $^{**}P = 0.003$; Sham vs. Vaccinated, $^{****}P < 0.0001$. NOTCH3 ECD deposits (number/1,000 μm^2): 3 m.o. vs. 18 m.o. $^{**}P = 0.0038$; 3 m.o. vs. 7 m.o. $^{***}P = 0.0002$; 7 m.o. vs. Sham, ns $P = 0.9913$; 7 m.o. vs. Vaccinated, $^{*}P = 0.021$; Sham vs. Vaccinated, $^{***}P = 0.001$. NOTCH3 ECD deposits size: 3 m.o. vs. 18 m.o. $^{*}P = 0.0215$; 3 m.o. vs. 7 m.o. $^{**}P = 0.0029$; 7 m.o. vs. Sham, ns $P = 0.3622$; 7 m.o. vs. Vaccinated, $^{*}P = 0.0428$; Sham vs. Vaccinated, $^{**}P = 0.0038$, ns = non-significant). Dotted lines indicate quartiles and dashed thicker lines are the median.
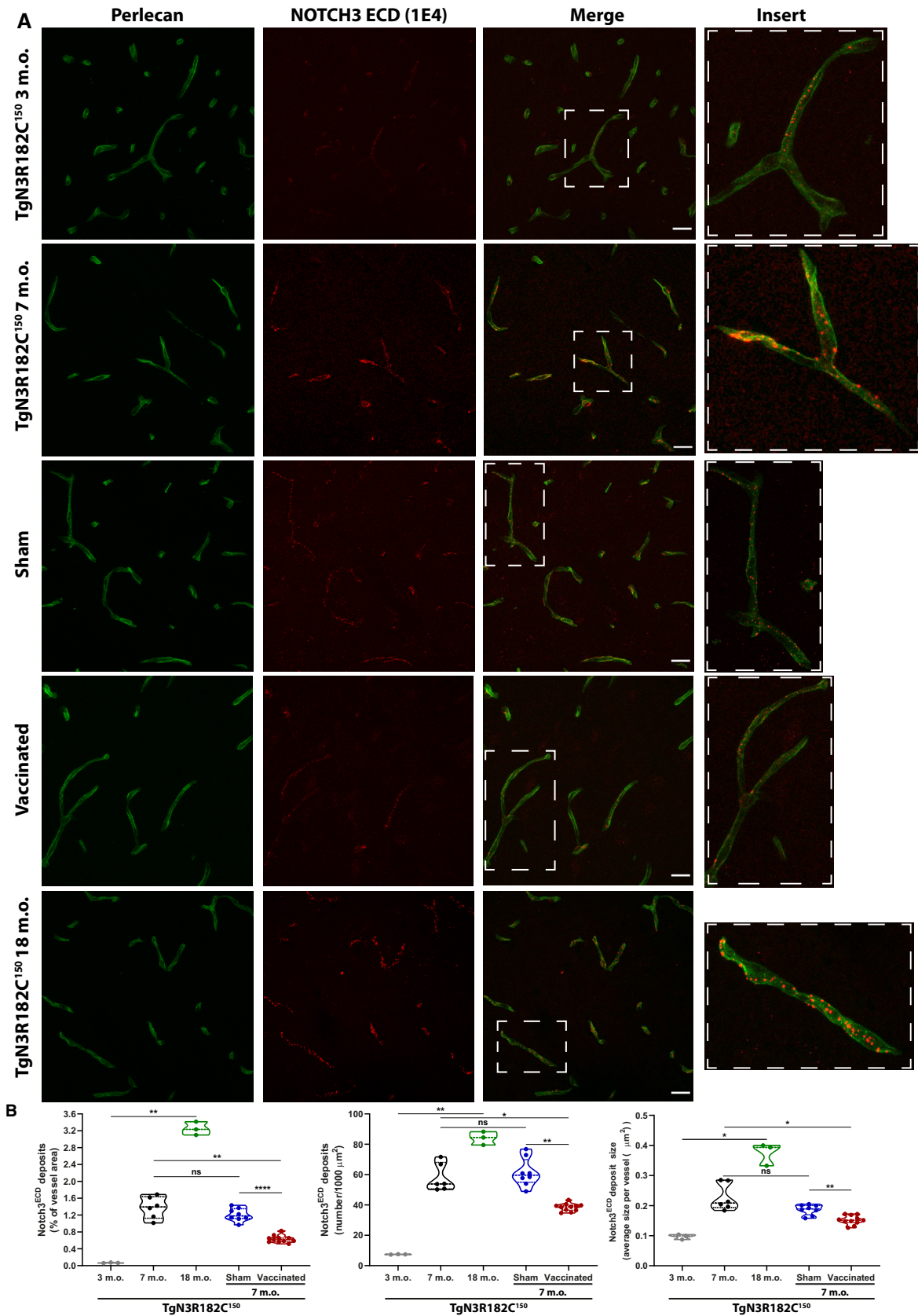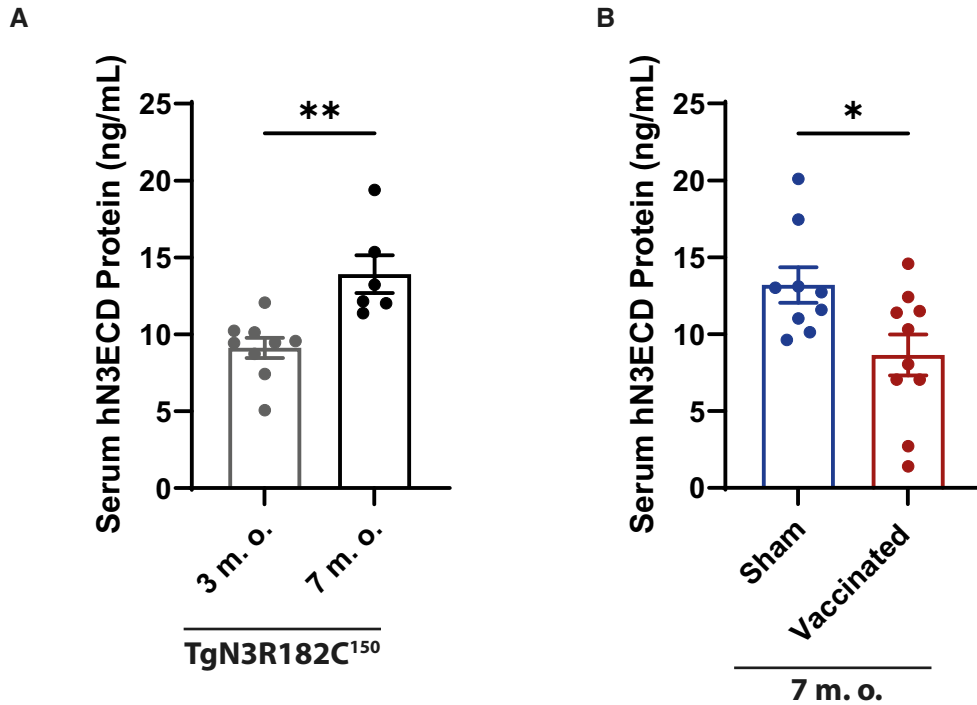
Source data are available online for this figure.

Figure 5.

Figure 6. Quantification of human NOTCH3 ECD protein present in whole blood serum of sham, immunized and non-vaccinated TgN3R182C150 mice (at 3 and 7 months old).

A   NOTCH3 ECD was detected in the whole blood serum of the non-treated TgN3R182C150 mice at 3 months ($n = 9$) of age and further increased at 7 months ($n = 6$) of age. Serum from Notch3$^{-/-}$ and C57Bl6/J WT mice were included as negative controls. Statistical analysis was performed using unpaired Student's t-test with Welch's correction (3 m.o. vs. 7 m.o. ***$P = 0.0005$). Error bars indicate standard error of the mean (SEM).

B   NOTCH3 ECD in the TgN3R182C150 mice was significantly reduced in the vaccinated ($n = 10$) TgN3R182C150 mice vs. sham ($n = 9$). Statistical analysis was performed using unpaired Student's t-test with Welch's correction (Sham vs. Vaccinated *$P = 0.0196$). Error bars indicate standard error of the mean (SEM).

Source data are available online for this figure.

et al, 2002). The reduced deposition of NOTCH3 aggregates in the capillaries of vaccinated TgN3R182C^{150} mice indicates that immune-mediated clearance of these aggregates may been activated, with microglia being a likely culprit. To address this, we performed immunostaining for activated microglia using Iba1 (expressed at low levels in resting microglia and at higher levels in activated and migrating microglia) and CD68 (expressed in activated microglia). Combined immunostaining for Iba1 and CD68 revealed an increase in the number of CD68-positive cells ($P = 0.0087$) as well as the area ($P = 0.0157$) in which they were localized in relation to Iba1-staining in 7-month-old vaccinated TgN3R182C^{150} mice compared with control or sham-vaccinated TgN3R182C^{150} mice (Fig 7A and B). There was also a trend towards more NOTCH3 ECD deposits inside or in close vicinity to microglia in vaccinated TgN3R182C^{150} mice compared with control or sham-vaccinated TgN3R182C^{150} mice, although the difference did not reach statistical significance

Figure 7. Microglia activation and NOTCH3 ECD expression in sham, immunized and non-vaccinated TgN3R182C150 mice at 7 months.

A   Representative images show microglia stained with anti-CD68 antibody (red) and Iba1 antibody (green). Scale bar = 20 μm.

B   Quantification of CD68-stained area revealed a significant increase in the % of microglia and microglia area between N3 EGF$_{1-5}$-immunized ($n = 6$), sham ($n = 4$), and non-vaccinated TgN3R182C150 ($n = 5$) mice. Statistical significance was assessed using an ordinary one-way ANOVA followed by Tukey's multiple comparisons test (% microglia with CD68 staining: 7 m.o. vs. Sham ns $P = 0.7393$; Sham vs. Vaccinated **$P = 0.0087$. CD68 staining (% of microglia area): 7 m.o. vs. Sham $P = 0.9131$; Sham vs. Vaccinated *$P = 0.0157$, ns = non-significant). Error bars indicate standard error of the mean (SEM).

C   Representative images of TgN3R182C150, sham-, and NOTCH3 EGF$_{1-5}$-immunized mice at 7 months of age stained with a monoclonal antibody against NOTCH3 ECD (1E4, red) and an antibody against microglia (Iba1, green). Scale bar = 20 μm.

D   Quantification of NOTCH3 ECD deposits (numbers per 1,000 μm^2) and NOTCH3 ECD stained area and average size per microglia revealed no alterations between the NOTCH3 EGF$_{1-5}$-immunized ($n = 11$), sham ($n = 8$), and non-vaccinated TgN3R182C150 ($n = 6$) mice at 7 months of age. Statistical significance was assessed using an ordinary one-way ANOVA followed by Tukey's multiple comparisons test (% microglia with NOTCH3 ECD deposits: 7 m.o. vs. Sham ns $P = 0.7997$; Sham vs. Vaccinated ns $P = 0.0526$. NOTCH3 ECD deposits (% of microglia area): 7 m.o. vs. Sham ns $P = 0.5362$; Sham vs. Vaccinated ns $P = 0.8059$. NOTCH3 ECD deposits (number/1,000 μm^2): 7 m.o. vs. Sham ns $P = 0.8392$; Sham vs. Vaccinated ns $P = 0.5777$. NOTCH3 ECD deposits size: 7 m.o. vs. Sham ns $P = 0.6664$; Sham vs. Vaccinated ns $P = 0.8787$, ns = non-significant). Error bars indicate standard error of the mean (SEM).
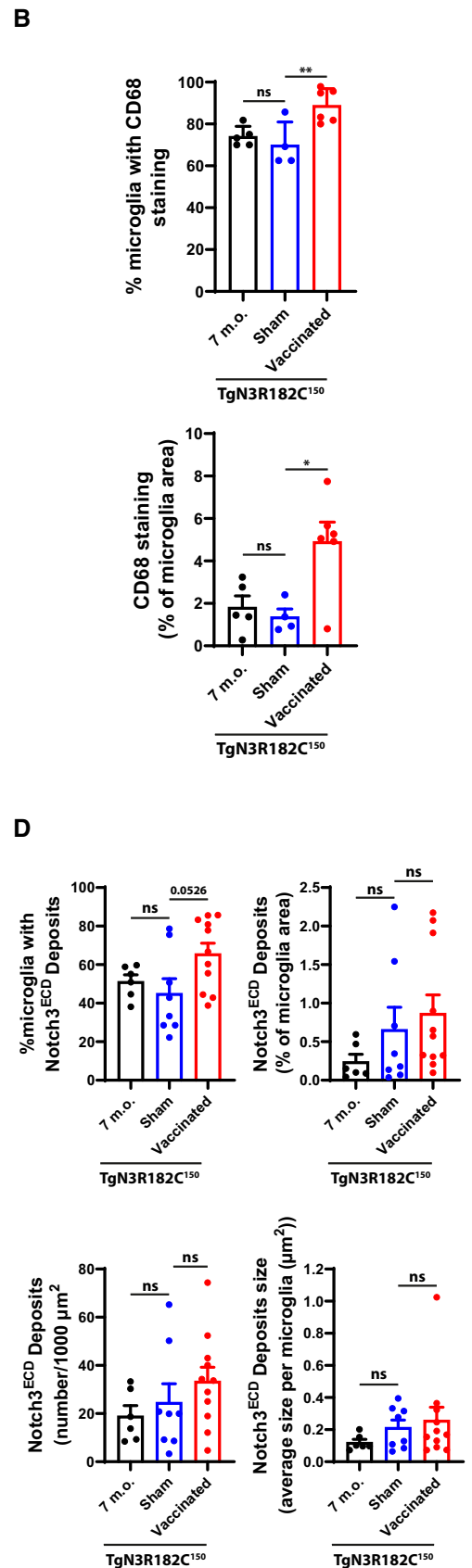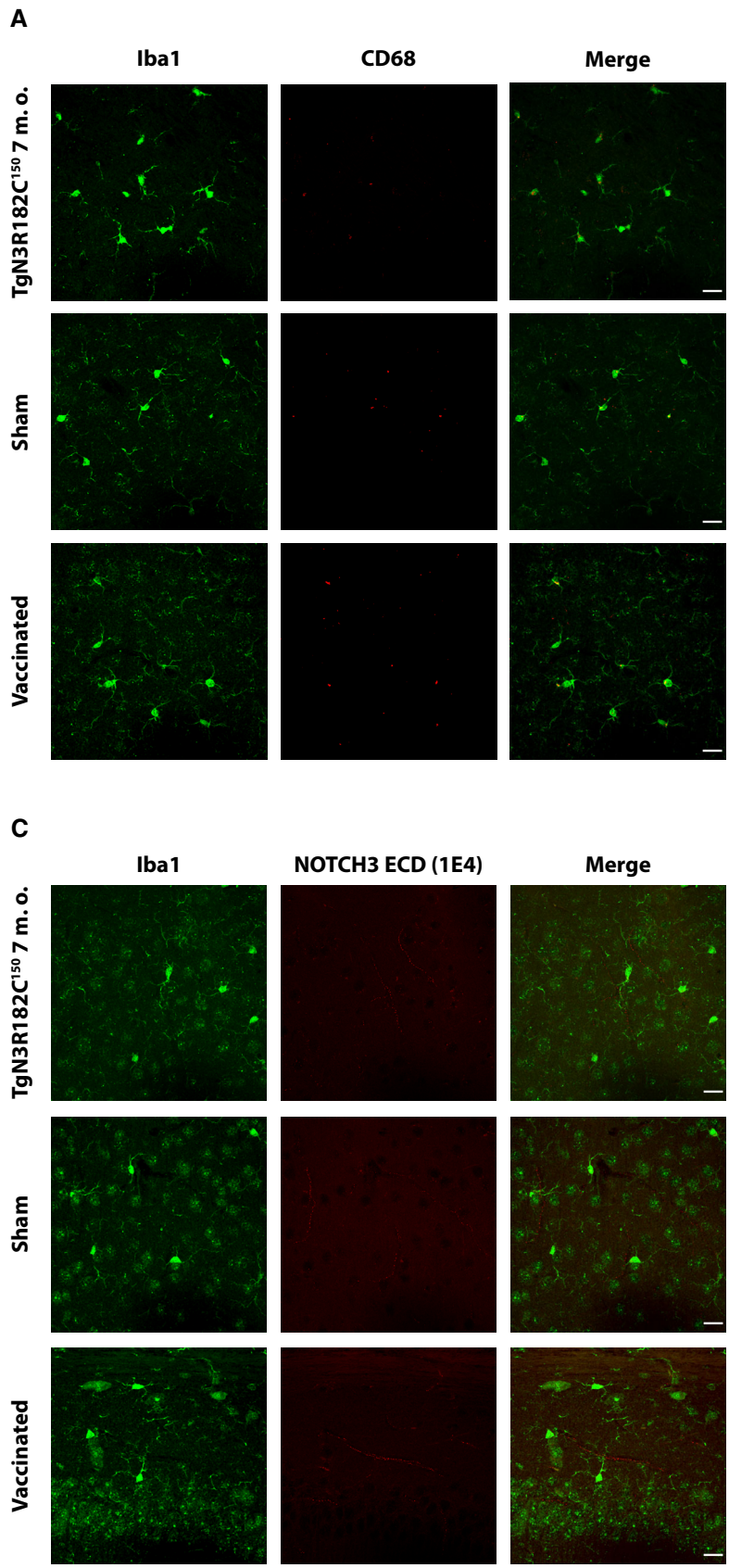
Source data are available online for this figure.

Figure 7.

(Fig 7C and D). In conclusion, the data suggest that active immunization with the NOTCH3 EGF_{1-5} WT/R133C aggregates increases the proportion of microglia with NOTCH3 deposits, while not changing the area or number of deposits within a microglial cell. Collectively, this may indicate an involvement of microglia in clearing the NOTCH3 ECD aggregates.

The number of retinal VSMC is not reduced by active immunization

Although the antibodies were generated towards NOTCH3 EGF_{1-5} aggregates, this does not exclude a potential targeting of NOTCH3 receptor function, which may disrupt NOTCH3 signaling and, in turn, cause adverse effects on the vasculature. The architecture of the retinal blood vessels is particularly amenable to analysis of vascular dysfunction as loss of NOTCH3 signaling in $Notch3^{-/-}$ mice leads to a progressive loss of VSMC in the retina (Henshall et al, 2015). We therefore wanted to establish whether active immunization with NOTCH3 EGF_{1-5} WT/R133C aggregates reduced the number of VSMC in retinal blood vessels as an indicator of whether NOTCH3 signaling was disturbed. Immunostaining for alpha-smooth muscle actin (ASMA) revealed no significant differences in the smooth muscle cell architecture of the retinal vasculature in control, vaccinated or sham-vaccinated TgN3R182C[150] mice compared with and WT (C57BL6/J) mice at 7 months of age (Fig 8A and B). In contrast, there was extensive loss of VSMC at 3 months of age in the $Notch3^{-/-}$ mice, compared with 3-month-old WT (C57BL6/J), in keeping with a previous report (Henshall et al, 2015; Fig 8C). Furthermore, the NOTCH3 EGF_{1-5} WT/R133C-vaccinated TgN3R182C[150] mice were normal with regard to body weight and general behavior (unpublished observation; Oliveira, Coupland). Together, this suggests that active immunization against NOTCH3 does not have a detrimental impact on NOTCH3 signaling.

Active immunization does not cause renal damage, inflammation, or neurodegeneration

To analyze whether the vaccination is safe and tolerable with regard to general tissue toxicity, we analyzed kidney morphology and architecture with hematoxyline/eosin staining and the presence of apoptotic cells by immunostaining for cleaved caspase 3. The staining revealed no differences between sham and vaccinated TgN3R182C[150] mice (Fig EV4A). Furthermore, to assess inflammation, we monitored the level of the inflammation marker C-reactive protein (CRP) in serum, and no significant differences between the sham and vaccinated mice were observed (Fig EV4B). Finally, to learn whether vaccination caused neuronal damage, neurofilament light chain protein in the serum was analyzed by a Single molecule array (Simoa) assay, and no significant difference was detected

between the sham and vaccinated TgN3R182C[150] mice (Fig EV4C). In conclusion, the absence of renal damage, inflammation and neurodegeneration suggests that vaccination with NOTCH3 EGF_{1-5} WT/R133C protein in TgN3R182C[150] mice is a safe and tolerable treatment therapy.

Discussion

Cerebral autosomal dominant arteriopathy with subcortical infarcts and leukoencephalopathy is the most common genetic form of small vessel disease but with no available therapies that can prevent, halt or cure the disease. There is thus a need to explore potential therapeutic strategies. In this report, we develop a novel active immunization strategy in a preclinical CADASIL model and demonstrate its ability to prevent NOTCH3 ECD aggregation, which is a key hallmark of CADASIL pathophysiology. We find that NOTCH3 ECD depositions around capillaries as well as NOTCH3 ECD levels in the blood are reduced in CADASIL mice treated with the NOTCH3 EGF_{1-5}-directed vaccine for 4 months and that the vaccine does not appear to interfere with the role of Notch signaling for vascular integrity or induce inflammation, neurodegeneration or kidney damage.

Several lines of evidence indicate that CADASIL pathology stems from aggregation of the NOTCH3 extracellular domain, and likely leads to disruption of the microarchitecture of the cerebrovasculature and ultimately reducing myogenic tone and resulting in a series of lacunar infarcts. Accumulation of NOTCH3 ECD is an early step in the pathogenic process, followed by formation of GOM deposits and the subsequent degeneration of the VSMC (Monet-Lepretre et al, 2013; Capone et al, 2016). To disrupt NOTCH3 misfolding and aggregation is therefore a promising therapeutic avenue to explore in CADASIL treatment. Immune-based therapies have become a leading and prioritized therapeutic strategy for other proteinopathies and neurodegenerative diseases during the past 20 years (Alpaugh & Cicchetti, 2019). In the quest for AD therapies, emerging encouraging results suggest a clinically meaningful effect from immunotherapies aimed at clearing Aβ-amyloid which recently also have led to the first FDA approval of a passive vaccine for treatment of AD (Golde et al, 2009; Demattos et al, 2012; Sevigny et al, 2016; Knopman et al, 2021).

Our data provide proof-of-principle that an active immunization strategy can reduce NOTCH3 aggregation in a pre-clinical model of CADASIL and thus may be beneficial also in the treatment of CADASIL. Active immunization against NOTCH3 accumulation using a 1:1 mixture of aggregated recombinantly expressed R133C (475T>C) and WT NOTCH3 EGF1-5 truncated protein fragments resulted in significantly reduced deposition of NOTCH3 aggregates in the capillaries of a transgenic CADASIL mouse model. The use of

Figure 8. The number of retinal VSMC is not reduced by active immunization.

A Immunostaining for smooth muscle actin (ASMA) revealed that there were no significant differences in the composition of the smooth muscle cell coating of vessels in the retinal vasculature in WT (C57Bl6/J) versus TgN3R182C150 mice at 7 months of age. Scale bar = 50 μm.

B Immunostaining for smooth muscle actin (ASMA) shows no significant differences in the composition of the smooth muscle cell coating of vessels in the retinal vasculature in NOTCH3 EGF_{1-5}-vaccinated versus sham-vaccinated TgN3R182C150 mice. Scale bar = 50 μm.

C Immunostaining for smooth muscle actin (ASMA) shows an extensive loss of VSMC in the Notch3$^{-/-}$ mice when compared with a WT (C57Bl6/J) at 3 months of age. Scale bar = 50 μm.
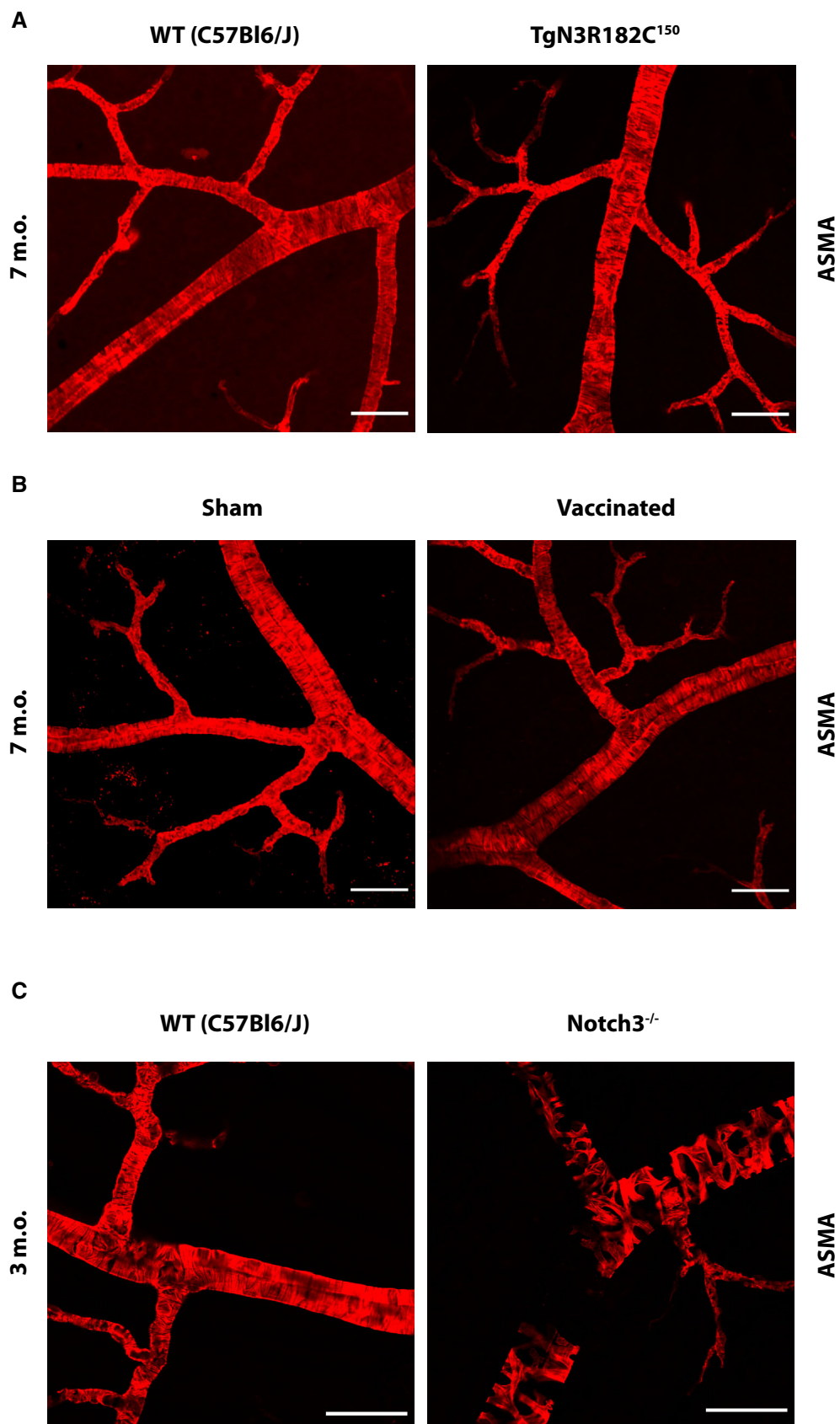
Figure 8.

NOTCH3 EGF$_{1-5}$ aggregates containing both mutant and WT NOTCH3 as the immunogen was selected as the vast majority of CADASIL patients are heterozygous mutation carriers and thus express both mutated and non-mutated NOTCH3, and it has been demonstrated that misfolded NOTCH3 ECD forms aggregates with WT NOTCH3 (Duering *et al*, 2011). It is thus reasonable to postulate that WT NOTCH3 co-aggregates with mutated misfolded NOTCH3 in CADASIL patients, and we noted that there appeared to be a more rapid formation of aggregates when both R133C and WT NOTCH3 ECD was present.

The reduction in NOTCH3 aggregation contrasts with observation from studies using a passive immunization approach. In one report, injection of the mouse monoclonal antibody (5E1) into a mouse model expressing the rat R169C *Notch3* CADASIL mutant revealed robust antibody binding to NOTCH3 aggregates in the brain, improved cerebral blood flow in response to acetylcholine or whisker stimulation, and restoration of myogenic tone of cerebral arteries (Ghezali *et al*, 2018). Interestingly, the amount of NOTCH3 aggregates or GOM was not reduced by 5E1 passive immunization, in contrast to the data presented in our study. Our study aimed to determine whether prevention of NOTCH3 aggregation occurred in a CADASIL model and did not investigate the capacity of the treatment to rescue vascular pathophysiology mainly due the absence of a CADASIL animal model that fully recapitulates the plethora of symptoms and pathologies seen in CADASIL. Another study was based on the use of an agonistic NOTCH3 antibody (A13) (Li *et al*, 2008) in a mouse model overexpressing C455R *NOTCH3* (Machuca-Parra *et al*, 2017), which generates a hypomorphic form of NOTCH3, leading to loss of VSMC. C455R NOTCH3 mice injected with A13 antibody showed a pronounced recovery of the VSMC coating of retinal vessels at 6 weeks of age, accompanied by a restoration of the decreased levels of NOTCH3 ECD in the blood of the C455R NOTCH3 mice (Machuca-Parra *et al*, 2017). While elegant, an agonist antibody strategy may however only be applicable to CADASIL mutations with hypomorphic signaling, such as C455R, whereas an active immunization strategy may target a broader set of CADASIL mutations, including the aggregation-prone R182C, which is signaling neutral (Fig EV5). To facilitate coverage of a broader set of mutations, we opted for using EGF$_{1-5}$ as an immunogenic agent, as it is the region of NOTCH3 containing most of the CADASIL-causing mutations identified thus far (Fig 1B). The fact that our immunization strategy, based on the use of NOTCH3 EGF$_{1-5}$ aggregates containing both WT and mutated NOTCH3, led to decreased NOTCH3 aggregation around cerebral capillaries and reduced serum levels of NOTCH3 ECD in a mouse model carrying a different *NOTCH3* mutation (R182C) suggests that active immunization with one mutant form can be efficient for CADASIL patients harboring different types of mutations. Such cross-mutation efficacy is of particular importance for the clinical translatability of a vaccine for CADASIL, as more than 200 cysteine-altering mutations have been identified and it would thus be infeasible to tailor a vaccine for each specific mutation.

The reduction in vascular NOTCH3 deposition was mirrored by reduced serum NOTCH3 ECD levels, providing further support for successful target engagement and suggesting that vascular and serum NOTCH3 levels are linked. This may be in line with a "peripheral sink" model, which posits that there is a passive equilibrium between aggregation-prone NOTCH3 in the blood and the brain, and that "capturing" of the protein in the blood would prevent deposition in the brain leading to less aggregation (DeMattos *et al*, 2002; Zhang & Lee, 2011). While theoretically appealing, the peripheral sink hypothesis seems unlikely to operate for Aβ aggregates in Alzheimer's disease (Georgievska *et al*, 2015; Honig *et al*, 2018), but it will be interesting to learn whether it may be a contender to explain the reduction of Notch3 ECD aggregates following active immunization.

We investigated whether microglia, the resident immune cells of the central nervous system, might be responsible for the reduction in NOTCH3 ECD aggregation in capillaries either by clearing aggregated NOTCH3 or by preventing its aggregation. We did not observe a significant volume of NOTCH3 ECD deposits within microglia, indicating that phagocytosis is likely not the main mechanism of NOTCH3 clearance, although it is possible that the lack of deposits may be a result of rapid turnover in the phagocytosis process. It is also possible that a peripheral humoral immune response leads to increased clearance of NOTCH3 prior to the formation of aggregates in the capillary bed.

As NOTCH3 signaling plays a pivotal role in vascular smooth muscle cell biology, it is important that NOTCH3-based CADASIL therapies do not affect Notch downstream signaling. Considering active immunization, we reasoned that targeting aggregated NOTCH3 ECD but not monomeric NOTCH3 would be important, and serum from immunized mice indeed showed a strong affinity for aggregated NOTCH3. In line with this, we noted a preserved VSMC coating in the retina, which indicates that endogenous Notch signaling was not affected by vaccination. In further support of a preference for aggregated NOTCH3, immunized mice did not display any abnormal behavior, obvious altered kidney morphology or function, neuronal degeneration or increased inflammation. The low levels of neurofilament light chain in the blood in the TgN3R182C[150] mice is in keeping with that magnetic resonance imaging (MRI) analysis of a more aggressive CADASIL mouse model (TgN3R182C[350]), which has higher NOTCH3 expression, revealed no difference when compared with controls at 20 months of age (Rutten *et al*, 2015; Gravesteijn *et al*, 2020). Together, these data suggest that vaccination with the NOTCH3 EGF$_{1-5}$ vaccine successfully targets NOTCH3 pathology in a tolerable manner.

It will be interesting to further investigate how our active immunization strategy might affect NOTCH3 deposition both long term and in older animals with advanced NOTCH3 aggregation. Our current study was designed to be a proof-of-principle study demonstrating that active immunization could indeed prevent NOTCH3 deposition. The next steps will be to determine whether it can reverse NOTCH3 deposition and whether being exposed to active vaccination for extended periods of time is safe. It will also be necessary to use a pre-clinical model of CADASIL that recapitulates the vascular physiology of the disease (i.e., decreased myogenic tone) to determine whether our therapeutic approach extends beyond NOTCH3 aggregate removal. For example, the CADASIL R169C mouse model, which exhibits reduced myogenic tone and cerebral blood flow, would be of interest to further explore our active therapeutic strategy (Joutel *et al*, 2010).

In conclusion, our study provides proof-of-principle that active immunization is an effective and tolerable therapy to reduce NOTCH3 ECD aggregates around capillaries and reduce NOTCH3 serum levels in a CADASIL mouse model. Given that inoculation with NOTCH3 from one CADASIL variant was capable of reducing aggregate load in another CADASIL variant, this active vaccination therapy could be applicable to a broad spectrum of CADASIL

variants. Thus, this study, providing the first demonstration of reduced vascular NOTCH3 pathology development, is a promising lead for the development of a CADASIL therapy.

Materials and Methods

Mouse maintenance, breeding, and genetics

TgN3R182C^{150} mice, which overexpress the full length human *NOTCH3* gene from a genomic BAC construct with the archetypal p.Arg182Cys mutation, were generated in a C57BL/6J genetic background purchased from Janvier Laboratories. Four mutant strains with different NOTCH3 RNA expression levels relative to endogenous mouse NOTCH3 RNA expression, including the TgN3R182C^{150} strain, were developed and have been previously described (Rutten *et al*, 2015). Mice were provided with water and food *ad libitum*, were maintained in a 12 h light/dark cycle, and housed in enriched cages. All experimental animal procedures were performed in accordance with local regulations and rules and according to ARRIVE guidelines were approved by the Stockholm Animal Ethics board (ethical permit no. 4433-2020).

Generation of stable HEK293 NOTCH3 EGF$_{1–5}$ WT and R133C cell lines

We used previously generated constructs encoding a truncated form of human NOTCH3 ECD (WT and R133C) consisting of the first five EGF-like repeats (N3 EGF$_{1–5}$, amino acids 1–234) with a poly-Histidine and c-Myc tags at the C-terminus (Duering *et al*, 2011). From these original constructs, we generated codon-optimized constructs using GeneArt gene synthesis (ThermoFisher) in the *piggyBac* transposon system to increase the yield of secreted protein. Human embryonic kidney 293 (HEK293) cells (ATCC), negative for mycoplasma contamination, were plated into 6-well plates (0.5×10^6 cells per well) and cultured in Dulbecco's modified Eagle's medium (DMEM; Invitrogen) supplemented with 10% fetal bovine serum (FBS; Invitrogen) and 1% penicillin–streptomycin (Invitrogen) at 37°C in a humidified 5% CO2 atmosphere. The following day 0.5 μg of NOTCH3 EGF$_{1–5}$ WT and R133C plasmids containing the *piggyBac* transposon and 0.2 μg of *piggyBac* transposase were transfected using Lipofectamine 2000 (Invitrogen) according to the manufacturer's instructions. Twenty-four hours after transfection, cells were split and selected for 2 weeks in DMEM medium containing 1 mg/ml of G418 (Invitrogen). After 2 weeks, the selected cells were expanded and maintained in DMEM medium with 0.6 mg/ml of G418.

Purification of NOTCH3 EGF$_{1–5}$ WT and R133C proteins

We purified NOTCH3 EGF$_{1–5}$ WT and R133C proteins as previously described (Oliveira *et al*, 2022). Briefly, HEK293 NOTCH3 EGF$_{1–5}$ WT and R133C (N3 EGF$_{1–5}$ WT and R133C) cells were grown in DMEM with 10% FBS until near confluency and were then washed with Dulbecco's phosphate-buffered saline (DPBS) and supplemented with DMEM medium without FBS for 5 days. The conditioned medium from both cell lines was collected, cleared from cell debris by centrifugation at 1,500 *g* and dialyzed with the aid of SnakeSkin Dialysis Tubing 10 KDa MWCO (ThermoFisher) in PBS for 24 h at 4°C. Dialyzed

medium from three flasks (~150 ml) of each cell line was equilibrated with 1 ml (bead volume) of cobalt ion affinity resin (TALON Superflow, GElifesciences) for 30 min with agitation at 4°C. Afterwards, the resin solution was added on a gravity flow column and washed three times with wash buffer (200 mM Sodium Phosphate buffer, 500 mM NaCl and 5 mM imidazole, at pH 7.5). After elution with elution buffer (200 mM Sodium Phosphate buffer, 500 mM NaCl and 300 mM imidazole, at pH 7.5), the fractions were pooled and dialyzed in a dialysis membrane (Spectrum™ Spectra/Por™ 1 6–8 KDa MWCO, Fisher Scientific) against PBS for 24 h at 4°C. The pooled fractions of the NOTCH3 EGF$_{1–5}$ WT and R133C were concentrated to 1 mg/ml in a concentration column (Vivaspin 6 10 KDa MWCO, Sartorius) according to the manufacturer's instructions. The protein concentration was measured with a BCA absorbance assay according to the manufacturer's instructions (Pierce™ BCA Protein Assay Kit #23225, ThermoFisher).

Immunization of TgN3R182C^{150} mice with aggregated NOTCH3 EGF$_{1–5}$ protein

NOTCH3 EGF$_{1–5}$ WT and NOTCH3 EGF$_{1–5}$ R133C proteins were incubated 1:1 to a final concentration of 0.5 mg/ml in PBS at 37°C for 5 days with gentle agitation (350 rpm), and the presence of aggregated NOTCH3 EGF$_{1–5}$ protein was verified using western blot and SDS–PAGE (Invitrogen) under non-reducing conditions. The aggregated NOTCH3 EGF$_{1–5}$ protein was mixed with the adjuvant or PBS to a concentration of 0.25 mg/ml. We performed the active immunization using a similar immunization schedule as Kontsekova and colleagues (Kontsekova *et al*, 2014) with slight modifications adjusted to using mouse rather than rat and the size of the immunized protein Briefly, 20 3-month-old transgenic TgN3R182C^{150} female and male mice were immunized initially either with 25 μg of aggregated NOTCH3 EGF$_{1–5}$ protein (*n* = 11, vaccinated) plus adjuvant (Imject Alum Adjuvant, ThermoFisher) or PBS (*n* = 9, sham) plus adjuvant, followed by a booster shot 4 weeks later containing 25 μg of aggregated NOTCH3 EGF$_{1–5}$ protein plus adjuvant and the corresponding sham booster shot. Subsequent booster shots of sham and aggregated NOTCH3 EGF$_{1–5}$ protein (25 μg) in PBS were performed every 2 weeks until a total of six immunization events have taken place over a period of 4 months.

Whole blood serum collection

Whole blood serum was collected from the immunized mice (*n* = 20), and non-immunized TgN3R182C^{150} at 3 months (*n* = 9) and 7 months (*n* = 6). Briefly, mice were anesthetized intraperitoneally with avertin (240 mg/kg) and blood was then collected from the right ventricle and dispensed to a tube with serum gel with clotting activator (Microvette 500 Z-Gel, Sarstedt). After centrifugation for 5 min at 10,000 *g*, the whole blood serum was collected, aliquoted, and stored at −80°C.

Antibody immune response titer validation of whole blood serum by ELISA

To detect the immune response of the immunization, we designed an indirect enzyme-linked immunosorbent assay (ELISA) against the NOTCH3 EGF$_{1–5}$ aggregates. Briefly, the plates were coated with

the antigen (NOTCH3 EGF$_{1-5}$ aggregates) at 0.625 µg/ml, followed by incubation overnight at 4°C. Blocking solution was added (PBS-T with 1% BSA and 10% goat serum) for 2 h at room temperature (RT). Next, the plates were washed two times with PBS, and the diluted whole blood serum samples of both sham and vaccinated mice were added to the plates followed by incubation overnight at 4°C. The following day, the plates were washed four times with PBS and incubated with polyclonal anti-mouse HRP conjugated secondary antibody (1:2,000) for 2 h at RT. After washing five times with PBS, the plates were incubated for 30 min with Pierce 1-Step Ultra TMB ELISA Substrate (ThermoFisher). Pre-warmed sulfuric acid stop solution (R&D Systems) at 37°C was used to stop the reaction and the absorbance was monitored at 450 nm with a Fluorostar galaxy plate reader.

NOTCH3 ECD custom ELISA

To detect NOTCH3 ECD in circulation, we designed an NOTCH3 ECD sandwich ELISA based on a previously described protocol (Primo et al, 2016). Briefly, high-affinity binding 96-well plates were coated with a NOTCH3 capture monoclonal antibody (MAB1559; R&D Systems) at 0.625 ng/µl in 100 µl of PBS and agitated overnight at 4°C. The plates were blocked for 3 h with agitation in a 10% BSA solution at RT. Whole blood serum samples were diluted 1:40 in 100 µl of reagent diluent (R&D Systems) and recombinant human NOTCH3 ECD (1559-NT-050; R&D Systems) was used as standard protein. The samples and standard were added to the plates and incubated with agitation overnight at 4°C. After three washes with washing buffer (R&D Systems), 100 µl of a solution containing 0.001 mg/ml of the detection biotinylated polyclonal antibody (R&D Systems) raised against NOTCH3 ECD and 2.5% BSA was added and was used for detection followed by agitation for 2 h at RT. The plates were washed three times with washing buffer and a horseradish peroxidase-streptavidin (HRP-Strep) complex (R&D Systems) diluted 1:25 in reagent diluent was added to the plates and incubated for 40 min with agitation. After incubation and washing five times, the plates were incubated for 30 min with Pierce 1-Step Ultra TMB ELISA Substrate (ThermoFisher). Pre-warmed sulfuric acid stop solution (R&D Systems) at 37°C was used to stop the reaction and absorbance at 450 nm was measured in a Fluorostar galaxy plate reader.

NOTCH3 ECD protein competitive ELISA assay

We employed the above described NOTCH3 ECD custom ELISA to test the competition of NOTCH3 ECD in circulation. Briefly, whole blood serum samples from TgN3R182C^{150} mice ($n = 4$) were diluted 1:1 with whole blood samples from sham- or vaccinated C57BL6/J WT mice, followed by the same procedure as above.

Brain and retina collection and histology

Mice were deeply anesthetized intraperitoneally with avertin (240 mg/kg) and transcardially perfused with 50 ml of DPBS followed by 50 ml of 4% paraformaldehyde (PFA). The brain and retinas were collected and were postfixed overnight in 4% PFA at 4°C. One hemisphere of the brain was paraffin-embedded and was sagittal serially sectioned in 5–10 µm sections and placed in positively charged slides.

Immunofluorescence analysis of isolated brain microvessels

Cerebral small vessels were isolated and purified as described (Boulay et al, 2015). In brief, the brain was taken out from an anesthetized mouse, the cerebellum and olfactory bulb were removed, choroid plexus and meninges were peeled away. Brain tissue was homogenized using a homogenizer, followed by gradient centrifugation. Microvessels were isolated and purified by passing through a 20 µm-mesh filter. Isolated microvessels were then seeded on Superfrost Plus slides and fixed with 4% formaldehyde followed by blocking using 2% BSA with 0.3% Triton-X in PBS and stained with antibodies of α-Smooth Muscle-Cy3 antibody (1:1,000, clone 1A4; Sigma-Aldrich), primary anti-Perlecan (1:300, clone A7L6; Millipore), anti-PDGFRβ (1:50, #3169; Cell Signaling Technology), anti-NG2 (1:100, MAB6689; R&D systems) followed by incubation with Alexa 488 conjugated anti-rabbit, Alexa 594 conjugated anti-rat secondary antibody (1:1,000, Life Technologies). Images were taken using Zeiss confocal 880.

Immunohistochemistry

Sections were deparaffinized in xylene two times during 5 min, followed by rehydration of the tissue through a series of graded alcohols [100% ethanol (2× for 3 min), 95% ethanol (1× for 3 min), 70% ethanol (1× for 3 min), and H$_2$O MQ (1× 3 min)]. Next, heat antigen retrieval was performed by submerging the slides in Diva Decloaker buffer (Biocare Medical) and placing them in a pressure cooker (Biocare Medical) for 30 min at 110°C. Slides were cooled at RT for 30 min and placed in PBS for 15 min on a shaker. Brain sections were outlined with a hydrophobic barrier using a PAP pen, and a permeabilization solution (PBS with 2% BSA and 0.3% Triton-X) was loaded onto the tissue for 10 min at RT. The tissues were then blocked for 30 min with Rodent Block M (Biocare Medical) followed by 30 min with blocking solution (PBS with 1% BSA and 10% goat serum). To assess the NOTCH3 ECD deposits, the tissues were incubated overnight at 4°C with mouse monoclonal anti-human NOTCH3 ECD primary antibody (1:100, clone 1E4, Millipore) followed by detection with Alexa 594 conjugated anti-mouse secondary antibody (1:1,000, Life Technologies). Capillaries were identified by immunostaining with rat monoclonal anti-perlecan antibody (1:100, clone A7L6, Millipore) overnight at 4°C followed by detection with Alexa 488 conjugated anti-rat secondary antibody (1:1,000, Life Technologies). Arteries were identified by immunostaining with a mouse monoclonal anti-actin, α-Smooth Muscle-FITC antibody (1:500, clone 1A4; Sigma-Aldrich) overnight at 4°C. Microglia were stained with a rat monoclonal anti-CD68 antibody (1:100, Bio-Rad) and with a rabbit monoclonal anti-Iba1 antibody (1:100, WAKO) overnight at 4°C followed by detection with Alexa 488 conjugated anti-rabbit secondary antibody (1:1,000, Life Technologies), and Alexa 594 conjugated anti-rat secondary antibody (1:1,000, Life Technologies). Stained sections were imaged at 63x magnification using a Zeiss LSM880 microscope. Images were captured with identical settings across sections. The entire procedure was performed under blinded conditions.

Quantification of NOTCH3 ECD deposits

The quantitative image analyses were performed blinded to the genotype and using pre-established parameters (ImageJ Software,

Fiji distribution) (Schindelin *et al*, 2012). We analyzed NOTCH3 ECD deposits on maximal intensity projections of image stacks by applying the following pipeline: (i) manual delineation of arteries and delineation of capillaries by automated segmentation on the perlecan channel, and subsequent creation of a region of interest (ROI) for each vessel followed by the measurement of the vessels area; (ii) on the NOTCH3 ECD channel the segmentation was achieved by performing automatic image thresholding (RenyiEntropy method), followed by automatic detection and counting of number and the area of NOTCH3 ECD deposits inside each ROI by using the "Analyze Particles" function of Fiji. To quantify the NOTCH3 ECD deposits, three nonadjacent sections (50 μm apart) were analyzed per mouse (10–14 images randomly selected per animal section). The mean of the randomly selected image fields (224.92 × 224.92 μm) per section was used to quantify NOTCH3 ECD load in capillaries and arteries. All vessels (capillaries and arteries) in the randomly selected image fields (224.92 × 224.92 μm) were included in the quantification of NOTCH3 ECD deposits as an ROI. The entire procedure was performed under blinded conditions. Results are represented as the number, average size and surface area of NOTCH3 ECD deposits on the vessel area.

Quantification of activated microglia

The quantitative image analysis was performed blinded to the genotype as described above. We analyzed the activated microglia on maximal intensity projections of image stacks by applying the following pipeline: (i) delineation of microglia by automated and manual segmentation on the Iba1 channel, and subsequent creation of a ROI for each microglia followed by the measurement of the microglia area; (ii) on the CD68 channel (activated microglia) the segmentation was achieved by performing automatic image thresholding (RenyiEntropy method), followed by automatic detection and counting of number and the area of CD68 staining inside each ROI by using the "Analyze Particles" function of Fiji. To quantify the activated microglia, three nonadjacent sections (50 μm apart) were analyzed per mouse (4–6 images randomly selected per animal section). The mean of the randomly selected image fields (224.92 × 224.92 μm) per section was used to quantify CD68 stain in the microglia area. All microglia in the randomly selected image fields (224.92 × 224.92 μm) were included in the quantification of activated microglia as an ROI. The % of microglia area represents the percentage that the CD68 staining (stained by Iba1) occupies per microglia area. To analyze the NOTCH3 ECD deposits that colocalize with the microglia area, we employed the same pipeline described above to select the microglia area in the Iba1 channel. We then measured the NOTCH3 ECD deposits in the ROI employing the same pipeline we used for measuring the load of NOTCH3 ECD deposits in the vessels. All microglia in the randomly selected image fields (224.92 × 224.92 μm) were included in the quantification of NOTCH3 ECD deposits as an ROI. The entire procedure was performed under blinded conditions. The results are represented as the number, average size, and surface area of NOTCH3 ECD deposits on the microglia area.

Immunostaining of whole mount retina

The mouse retinas were dissected and removed from the eyecups and washed three times in PBS at RT for 5 min, followed by permeabilization in 0.3% Triton X-100 in PBS and blocked in PBS with 2% BSA and 10% goat serum for 2 h at RT. Retinas were then incubated for 24 h at 4°C with primary antibodies diluted in PBS containing 3% BSA, 0.1% Triton and with secondary antibodies diluted in the same buffer. After washes with 0.1% Triton X-100/PBS, retinas were flat mounted and imaged using a Zeiss LSM880 microscope.

Hematoxylin and eosin (H&E) staining and immunohistochemistry of paraffin-embedded kidney sections

Slides of 5 μm kidney paraffin sections from two sham and two vaccinated mice were first deparaffinized as described (Rodig, 2021) followed by staining with hematoxylin for 6 min and rinsing with water for 3 min. Next, to enhance staining contrast between tissues, the slides were treated with 1% HCl in 70% alcohol for 30 s and bluing of the nuclei was achieved with 0.1% NaOH for 1 min. After rinsing with water, sections were stained with eosin for 30 s. Slides were then washed and dehydrated with graded alcohol (i.e., 70, 95, and 100%) and xylene for 1 min each then mounted with DPX mounting media (Sigma-Aldrich). Images were taken at 200× magnification on a Nikon eclipse E800 microscope and analyzed using ImageJ software.

For immunohistochemistry analysis of cleaved caspase 3, deparaffinized sections were further subjected to heat antigen retrieval by submerging the slides into Diva Decloaker buffer (Biocare Medical) in a pressure cooker (Biocare Medical) for 30 min at 105°C. Sections were rinsed in PBS and endogenous peroxidases were blocked with Peroxidazed 1 (Biocare Medical) for 5 min. After rinsing with PBS, the slides were incubated with Background SNIPER (Biocare Medical) for 10 min and rinsed with PBS. Sections were incubated with rabbit-anti-cleaved caspase-3 antibody (1:300, #9661; Cell Signaling Technology) followed by incubation with March3 Rabbit HRP-Polymer Detection (Biocare Medical). The samples were then washed with PBS and developed using DAB (Biocare Medical) for 5 min, rinsed thoroughly with water, counter stained with hematoxylin for 2 min and mounted with DPX. Images were taken at 200× magnification on a Nikon eclipse E800 microscope and analyzed using ImageJ software.

C-reactive protein (CRP) measurement

To assay the CRP concentrations in mouse serum, samples were diluted 1:300 and measured using a Mouse C-Reactive Protein ELISA Kit according to the protocol provided by the manufacturer (ab222511, Abcam). The quantity of CRP was interpolated from a standard curve.

Neurofilament light chain measurement

Neurofilament light chain concentration was measured using the commercially available Simoa NF-Light assay on an HD-X analyzer according to instructions from the kit manufacturer (Quanterix, Billerica, MA). The measurements were performed by board-certified laboratory technicians who were blinded to the genetic or treatment background of the animals. The measurements were performed in one round using one batch of reagents. Calibrators were run in duplicates and outlier calibrator replicates were masked before curve fitting. Samples were run in singlicates at an 8-fold dilution.

The paper explained

Problem

Cerebral autosomal dominant arteriopathy with subcortical infarcts and leukoencephalopathy (CADASIL) is a disease affecting the blood vessels of the brain. Patients suffering from CADASIL experience migraine with aura, strokes and cognitive decline. CADASIL is caused by mutations in a specific gene, NOTCH3, and is currently incurable with no therapies in clinical use.

Results

We have developed an active immunization approach aimed at targeting the CADASIL-associated NOTCH3 pathology and assessed efficacy in a transgenic mouse model for CADASIL. We find that active repeated immunization with a short CADASIL-mutated NOTCH3 peptide resulted in reduced deposition of the extracellular domain of the NOTCH3 receptor around the smallest vessels in the brain (capillaries) and reduced levels of NOTCH3 extracellular domain in the blood in the CADASIL mouse model. There were no signs of kidney toxicity, inflammation, neurodegeneration or loss of vascular smooth muscle cells in the vasculature in the immunized mice.

Impact

Cerebral autosomal dominant arteriopathy with subcortical infarcts and leukoencephalopathy is a dominant disease, meaning that individuals carrying a CADASIL NOTCH3 mutation will develop the disease, and the fact that there are yet no functional therapies for CADASIL fuels efforts to explore novel therapy strategies. Our finding that active immunization reduces accumulation of the NOTCH3 extracellular domain around capillaries in the brain of a CADASIL mouse model is therefore encouraging. Importantly, the finding that immunization does not alter normal Notch signaling nor lead to kidney damage indicates that active immunotherapy may be an efficacious and tolerable therapeutic strategy for CADASIL therapy development.

For quality control (QC) sample with a concentration of 7.04 pg/ml, repeatability was 8.47%. For a QC sample with a concentration of 40.3 pg/ml, repeatability was 11.2%.

Luciferase assay

NIH3T3 cells (ATCC), negative for mycoplasma contamination, were transfected with $12 \times$ CSL-luc and CMV-β-galactosidase plasmids together with *NOTCH3* wild-type, R182C plasmid, or pcDNA3 vector as a control. Five hours post-transfection, cells were seeded on ligand Jag2 or Fc coated plates and DMSO as a vehicle and the γ-secretase inhibitor DAPT (10 μM) were added overnight. After incubation for 24 h, the cells were lysed in Cell culture lysis reagent (Promega) and luciferase activity was measured in duplicate by the GloMax® Multi Detection System apparatus (Promega) using the Dual-Glo Luciferase Assay System (Promega) according to the manufacturer's protocol. In all assays, relative luciferase activity was calculated as the ratio of Luciferase values normalized to β-gal levels.

Quantitative real-time PCR analysis

Brain vessels were isolated as previously described (Matthes *et al*, 2021), followed by RNA extraction using RNeasy mini kit (QIAGEN) and cDNA synthesis with Maxima First Strand cDNA Synthesis Kit (ThermoFisher Scientific). Real-time PCR analysis was performed using the Applied Biosystems 7500 Fast Real-Time PCR System

according to the manufacturer's protocol. The primers for qPCR are Hes1: forward 5′-CCAGCCAGTGTCAACACGA-3′, reverse 5′-AAT GCCGGGAGCTATCTTTCT-3′; Hey1: forward 5′-CCCCTCACCCTAC TCACCA-3′, reverse 5′-GCTTCAACCCAGACCCAA-3′; Nrip2: forward 5′- GGGAAGAATGTGTGGAGTGG-3′, reverse 5′-GAAGGCAGCAATG AAGAAGC-3′; NOTCH3: forward 5′-GAAGTTACCCCCAAGAGGC AA, reverse 5′-TATCTCGGTCACGCTGCAA-3′.

Statistical analysis

GraphPad Prism 9 was used to generate the graphs, All results are presented as mean ± standard error of the mean (SEM). Shapiro–Wilk normality and log normality and F tests were performed before choosing the statistical test to apply. Student's *t*-test with Welch's correction was used to assess the statistical differences between experimental groups. Multiple comparisons were evaluated by 1-way analysis of variance (ANOVA) followed by Brown–Forsythe and Welch ANOVA tests and followed by Dunnett's T3 multiple comparisons test in cases where different groups did not have equal variance. $P < 0.05$ was considered significant (*$P < 0.05$, **$P < 0.01$, ***$P < 0.001$, ****$P < 0.0001$). All exact P-values are listed in the supplemental Appendix Table S1.

Data availability

We have no data that require deposition in a public database.

Expanded View for this article is available online.

Author contributions

Daniel V Oliveira: Data curation; software; formal analysis; investigation; visualization; methodology; writing – original draft; writing – review and editing. **Kirsten G Coupland:** Data curation; software; formal analysis; investigation; visualization; methodology; writing – original draft; writing – review and editing. **Wenchao Shao:** Data curation; formal analysis; investigation; methodology; writing – review and editing. **Shaobo Jin:** Data curation; formal analysis; investigation; visualization; methodology; writing – review and editing. **Francesca Del Gaudio:** Data curation; software; formal analysis; investigation; visualization; methodology; writing – original draft; writing – review and editing. **Sailan Wang:** Formal analysis; investigation; writing – review and editing. **Rhys Fox:** Investigation; writing – review and editing. **Julie W Rutten:** Methodology; writing – review and editing. **Johan Sandin:** Conceptualization; writing – review and editing. **Henrik Zetterberg:** Resources; formal analysis; validation; investigation; methodology; writing – review and editing. **Johan Lundkvist:** Conceptualization; resources; supervision; funding acquisition; validation; writing – original draft; writing – review

and editing. **Saskia AJ Lesnik Oberstein:** Resources; validation; methodology; writing – review and editing. **Urban Lendahl:** Conceptualization; resources; supervision; funding acquisition; validation; writing – original draft; project administration; writing – review and editing. **Helena Karlström:** Conceptualization; resources; supervision; funding acquisition; validation; writing – original draft; project administration; writing – review and editing.

Disclosure and competing interests statement

References

Alpaugh M, Cicchetti F (2019) A brief history of antibody-based therapy. *Neurobiol Dis* 130: 104504

Andersson ER, Sandberg R, Lendahl U (2011) Notch signaling: simplicity in design, versatility in function. *Development* 138: 3593–3612

Boulay AC, Saubamea B, Decleves X, Cohen-Salmon M (2015) Purification of mouse brain vessels. *J Vis Exp* e53208

Budd Haeberlein S, O'Gorman J, Chiao P, Bussiere T, von Rosenstiel P, Tian Y, Zhu Y, von Hehn C, Gheuens S, Skordos L *et al* (2017) Clinical development of aducanumab, an anti-Abeta human monoclonal antibody being investigated for the treatment of early Alzheimer's disease. *J Prev Alzheimers Dis* 4: 255–263

Capone C, Cognat E, Ghezali L, Baron-Menguy C, Aubin D, Mesnard L, Stohr H, Domenga-Denier V, Nelson MT, Joutel A (2016) Reducing Timp3 or vitronectin ameliorates disease manifestations in CADASIL mice. *Ann Neurol* 79: 387–403

Chabriat H, Joutel A, Dichgans M, Tournier-Lasserve E, Bousser MG (2009) Cadasil. *Lancet Neurol* 8: 643–653

Coupland K, Lendahl U, Karlstrom H (2018) Role of NOTCH3 mutations in the cerebral small vessel disease cerebral autosomal dominant arteriopathy with subcortical infarcts and leukoencephalopathy. *Stroke* 49: 2793–2800

DeMattos RB, Bales KR, Cummins DJ, Paul SM, Holtzman DM (2002) Brain to plasma amyloid-beta efflux: a measure of brain amyloid burden in a mouse model of Alzheimer's disease. *Science* 295: 2264–2267

Demattos RB, Lu J, Tang Y, Racke MM, Delong CA, Tzaferis JA, Hole JT, Forster BM, McDonnell PC, Liu F *et al* (2012) A plaque-specific antibody clears existing beta-amyloid plaques in Alzheimer's disease mice. *Neuron* 76: 908–920

Duering M, Karpinska A, Rosner S, Hopfner F, Zechmeister M, Peters N, Kremmer E, Haffner C, Giese A, Dichgans M *et al* (2011) Co-aggregate formation of CADASIL-mutant NOTCH3: a single-particle analysis. *Hum Mol Genet* 20: 3256–3265

Forman MS, Trojanowski JQ, Lee VM (2004) Neurodegenerative diseases: a decade of discoveries paves the way for therapeutic breakthroughs. *Nat Med* 10: 1055–1063

Georgievska B, Gustavsson S, Lundkvist J, Neelissen J, Eketjall S, Ramberg V, Bueters T, Agerman K, Jureus A, Svensson S *et al* (2015) Revisiting the peripheral sink hypothesis: inhibiting BACE1 activity in the periphery does not alter beta-amyloid levels in the CNS. *J Neurochem* 132: 477–486

Ghezali L, Capone C, Baron-Menguy C, Ratelade J, Christensen S, Ostergaard Pedersen L, Domenga-Denier V, Pedersen JT, Joutel A (2018) Notch3(ECD) immunotherapy improves cerebrovascular responses in CADASIL mice. *Ann Neurol* 84: 246–259

Golde TE, Das P, Levites Y (2009) Quantitative and mechanistic studies of Abeta immunotherapy. *CNS Neurol Disord Drug Targets* 8: 31–49

Gravesteijn G, Munting LP, Overzier M, Mulder AA, Hegeman I, Derieppe M, Koster AJ, van Duinen SG, Meijer OC, Aartsma-Rus A *et al* (2020) Progression and classification of granular osmiophilic material (GOM) deposits in functionally characterized human NOTCH3 transgenic mice. *Transl Stroke Res* 11: 517–527

Henshall TL, Keller A, He L, Johansson BR, Wallgard E, Raschperger E, Mae MA, Jin S, Betsholtz C, Lendahl U (2015) Notch3 is necessary for blood vessel integrity in the central nervous system. *Arterioscler Thromb Vasc Biol* 35: 409–420

Honig LS, Vellas B, Woodward M, Boada M, Bullock R, Borrie M, Hager K, Andreasen N, Scarpini E, Liu-Seifert H *et al* (2018) Trial of solanezumab for mild dementia due to Alzheimer's disease. *N Engl J Med* 378: 321–330

Joutel A (2020) Prospects for diminishing the impact of nonamyloid small-vessel diseases of the brain. *Annu Rev Pharmacol Toxicol* 60: 437–456

Joutel A, Corpechot C, Ducros A, Vahedi K, Chabriat H, Mouton P, Alamowitch S, Domenga V, Cecillion M, Marechal E *et al* (1996) Notch3 mutations in CADASIL, a hereditary adult-onset condition causing stroke and dementia. *Nature* 383: 707–710

Joutel A, Favrole P, Labauge P, Chabriat H, Lescoat C, Andreux F, Domenga V, Cecillon M, Vahedi K, Ducros A *et al* (2001) Skin biopsy immunostaining with a Notch3 monoclonal antibody for CADASIL diagnosis. *Lancet* 358: 2049–2051

Joutel A, Monet-Lepretre M, Gosele C, Baron-Menguy C, Hammes A, Schmidt S, Lemaire-Carrette B, Domenga V, Schedl A, Lacombe P *et al* (2010) Cerebrovascular dysfunction and microcirculation rarefaction precede white matter lesions in a mouse genetic model of cerebral ischemic small vessel disease. *J Clin Invest* 120: 433–445

Karlstrom H, Beatus P, Dannaeus K, Chapman G, Lendahl U, Lundkvist J (2002) A CADASIL-mutated Notch 3 receptor exhibits impaired intracellular trafficking and maturation but normal ligand-induced signaling. *Proc Natl Acad Sci USA* 99: 17119–17124

Knopman DS, Jones DT, Greicius MD (2021) Failure to demonstrate efficacy of aducanumab: an analysis of the EMERGE and ENGAGE trials as reported by Biogen, December 2019. *Alzheimers Dement* 17: 696–701

Kontsekova E, Zilka N, Kovacech B, Novak P, Novak M (2014) First-in-man tau vaccine targeting structural determinants essential for pathological tau-tau interaction reduces tau oligomerisation and neurofibrillary degeneration in an Alzheimer's disease model. *Alzheimers Res Ther* 6: 44

Li K, Li Y, Wu W, Gordon WR, Chang DW, Lu M, Scoggin S, Fu T, Vien L, Histen G *et al* (2008) Modulation of Notch signaling by antibodies specific for the extracellular negative regulatory region of NOTCH3. *J Biol Chem* 283: 8046–8054

Machuca-Parra AI, Bigger-Allen AA, Sanchez AV, Boutabla A, Cardona-Velez J, Amarnani D, Saint-Geniez M, Siebel CW, Kim LA, D'Amore PA *et al* (2017) Therapeutic antibody targeting of Notch3 signaling prevents mural cell loss in CADASIL. *J Exp Med* 214: 2271–2282

Matthes F, Matuskova H, Arkelius K, Ansar S, Lundgaard I, Meissner A (2021) An improved method for physical separation of cerebral vasculature and parenchyma enables detection of blood-brain-barrier dysfunction. *NeuroSci* 2: 59–74

Mintun MA, Lo AC, Duggan Evans C, Wessels AM, Ardayfio PA, Andersen SW, Shcherbinin S, Sparks J, Sims JR, Brys M *et al* (2021) Donanemab in early Alzheimer's disease. *N Engl J Med* 384: 1691–1704

Monet-Lepretre M, Haddad I, Baron-Menguy C, Fouillot-Panchal M, Riani M, Domenga-Denier V, Dussaule C, Cognat E, Vinh J, Joutel A (2013) Abnormal recruitment of extracellular matrix proteins by excess Notch3 ECD: a new pathomechanism in CADASIL. *Brain* 136: 1830–1845

Novak P, Zilka N, Zilkova M, Kovacech B, Skrabana R, Ondrus M, Fialova L, Kontsekova E, Otto M, Novak M (2019) AADvac1, an active immunotherapy for Alzheimer's disease and non Alzheimer tauopathies: an overview of preclinical and clinical development. *J Prev Alzheimers Dis* 6: 63–69

Oliveira DV, Svensson J, Zhong X, Biverstal H, Chen G, Karlstrom H (2022) Molecular chaperone BRICHOS inhibits CADASIL-mutated NOTCH3 aggregation in vitro. *Front Mol Biosci* 9: 812808

Opherk C, Duering M, Peters N, Karpinska A, Rosner S, Schneider E, Bader B, Giese A, Dichgans M (2009) CADASIL mutations enhance spontaneous multimerization of NOTCH3. *Hum Mol Genet* 18: 2761–2767

Primo V, Graham M, Bigger-Allen AA, Chick JM, Ospina C, Quiroz YT, Manent J, Gygi SP, Lopera F, D'Amore PA et al (2016) Blood biomarkers in a mouse model of CADASIL. *Brain Res* 1644: 118–126

Rodig SJ (2021) Preparing paraffin tissue sections for staining. *Cold Spring Harb Protoc* 2021: pdb.prot099663

Rogers J, Strohmeyer R, Kovelowski CJ, Li R (2002) Microglia and inflammatory mechanisms in the clearance of amyloid beta peptide. *Glia* 40: 260–269

Rosenberg RN, Lambracht-Washington D (2020) Active immunotherapy to prevent Alzheimer disease-a DNA amyloid beta 1-42 trimer vaccine. *JAMA Neurol* 77: 289–290

Rutten JW, Haan J, Terwindt GM, van Duinen SG, Boon EM, Lesnik Oberstein SA (2014) Interpretation of NOTCH3 mutations in the diagnosis of CADASIL. *Expert Rev Mol Diagn* 14: 593–603

Rutten JW, Klever RR, Hegeman IM, Poole DS, Dauwerse HG, Broos LA, Breukel C, Aartsma-Rus AM, Verbeek JS, van der Weerd L et al (2015) The NOTCH3 score: a pre-clinical CADASIL biomarker in a novel human genomic NOTCH3 transgenic mouse model with early progressive vascular NOTCH3 accumulation. *Acta Neuropathol Commun* 3: 89

Rutten JW, Dauwerse HG, Gravesteijn G, van Belzen MJ, van der Grond J, Polke JM, Bernal-Quiros M, Lesnik Oberstein SA (2016) Archetypal NOTCH3 mutations frequent in public exome: implications for CADASIL. *Ann Clin Transl Neurol* 3: 844–853

Schindelin J, Arganda-Carreras I, Frise E, Kaynig V, Longair M, Pietzsch T, Preibisch S, Rueden C, Saalfeld S, Schmid B et al (2012) Fiji: an open-source platform for biological-image analysis. *Nat Methods* 9: 676–682

Sevigny J, Chiao P, Bussiere T, Weinreb PH, Williams L, Maier M, Dunstan R, Salloway S, Chen T, Ling Y et al (2016) The antibody aducanumab reduces Abeta plaques in Alzheimer's disease. *Nature* 537: 50–56

Shrivastava AN, Aperia A, Melki R, Triller A (2017) Physico-pathologic mechanisms involved in neurodegeneration: misfolded protein-plasma membrane interactions. *Neuron* 95: 33–50

Siebel C, Lendahl U (2017) Notch signaling in development, tissue homeostasis, and disease. *Physiol Rev* 97: 1235–1294

Tolar M, Abushakra S, Hey JA, Porsteinsson A, Sabbagh M (2020) Aducanumab, gantenerumab, BAN2401, and ALZ-801-the first wave of amyloid-targeting drugs for Alzheimer's disease with potential for near term approval. *Alzheimers Res Ther* 12: 95

Vandenberghe R, Riviere ME, Caputo A, Sovago J, Maguire RP, Farlow M, Marotta G, Sanchez-Valle R, Scheltens P, Ryan JM et al (2017) Active Abeta immunotherapy CAD106 in Alzheimer's disease: a phase 2b study. *Alzheimers Dement (N Y)* 3: 10–22

Vanlandewijck M, He L, Mae MA, Andrae J, Ando K, Del Gaudio F, Nahar K, Lebouvier T, Lavina B, Gouveia L et al (2018) A molecular atlas of cell types and zonation in the brain vasculature. *Nature* 554: 475–480

Yamamoto Y, Craggs LJ, Watanabe A, Booth T, Attems J, Low RW, Oakley AE, Kalaria RN (2013) Brain microvascular accumulation and distribution of the NOTCH3 ectodomain and granular osmiophilic material in CADASIL. *J Neuropathol Exp Neurol* 72: 416–431

Zhang Y, Lee DH (2011) Sink hypothesis and therapeutic strategies for attenuating Abeta levels. *Neuroscientist* 17: 163–173